The 7th International Supercritical CO_2 Power Cycles Symposium
February 21 – 24, 2022, San Antonio, Texas
Paper #198

Silicon Carbide Multilayer Piping for High Temperature sCO_2 Brayton Cycle

Jeff Halfinger
CEO and General Manager
Ceramic Tubular Products, LLC (CTP)
Lynchburg, VA

Jacob Neiderer
Research Engineer
Ceramic Tubular Products, LLC (CTP)
Lynchburg, VA

Dr. Farhad Mohammadi
Principal Engineer
Ceramic Tubular Products, LLC (CTP)
Lynchburg, VA

Kristen Frey
Research Engineer
Ceramic Tubular Products, LLC (CTP)
Lynchburg, VA

Dr. John Podhiny
Director
Materials Research & Design, Inc. (MR&D)
Wayne, Pa

Craig Iwano
Director
Materials Research & Design, Inc. (MR&D)
Wayne, Pa

Dr. Matthew Walker
Principal Member Technical Staff
Sandia National Laboratories (SNL)
Livermore, CA

Jeffrey Halfinger, CEO and General Manager, Ceramic Tubular Products, LLC (CTP)

Mr. Jeff Halfinger has a B.S., Metallurgical Engineering with over 35 years of experience in design and manufacturing engineering and program management, and business development. Mr. Halfinger served as Vice President and Chief Technology Officer at Babcock and Wilcox and Director of Defense Products at NovaTech before assuming the position of CEO and General Manager at CTP.

Jacob Neiderer, Research Engineer, Ceramic Tubular Products, LLC (CTP)

Mr. Jacob Neiderer obtained a B.S., Packaging Systems and Design at Virginia Tech. After working at BMW Manufacturing as a contracted project manager, Mr. Neiderer joined the CTP team to further the development of its high temperature SiC multilayer piping technology. Mr. Neiderer currently serves as the Principal Investigator on a Phase II SBIR – "Multilayer SiC Piping for 900°C sCO_2 Brayton Cycle".

Farhad Mohammadi-Koumleh, Ph.D., Principal Engineer, Ceramic Tubular Products, LLC (CTP)

Dr. Mohammadi received a Ph.D. in Materials Science and Engineering from Rutgers University, following two master degrees in Electronic Ceramics and Materials Science and Engineering from Rutgers and University of Florida, respectively. Dr. Mohammadi has 15 years of experience in the development of ceramic fibers, patented a high-volume production method of boron carbide fiber, and published numerous fiber-related articles in peer-reviewed journals. His work has led to two R&D100 awards, enlisting in Navy Success Stories, and several recognitions from the Department of Defense.

Kristen Frey, Research Engineer, Ceramic Tubular Products, LLC (CTP)

Ms. Kristen Frey received a B.S., Engineering Science from Sweet Briar College. She led several research projects on the use of multilayer, hybrid composite SiC tubes for various energy and industrial applications.

John Podhiny, Ph.D., Director, Materials Research & Design, Inc. (MR&D)

Dr. Podhiny has a B.S., M.S., and Ph.D. in Mechanical Engineering from Villanova University and over 20 years of experience in thermal-structural design and analysis, with an emphasis on advanced finite element modeling. His work typically focuses on high-temperature composite materials and utilizes fundamental micromechanics together with a range of finite element analysis (FEA) methods. Recent efforts have included the development of a standalone 3D FEA code for property predictions of fiber-reinforced composites and numerous customized FEA modules for Abaqus.

Craig Iwano, Director, Materials Research & Design, Inc. (MR&D)

Mr. Craig Iwano received both a B.E. and M.S. in Mechanical Engineering from Villanova University. He has over 18 years of experience in the design and analysis of complex structures for extreme environment applications, including composite control surfaces, load bearing thermal protection systems (TPS), rocket nozzles, structural insulators and impact resistant ceramic matrix composites (CMCs).

Matthew Walker, Ph.D., Principal Member Technical Staff, Sandia National Laboratories California (SNL)

Dr. Walker received a M.S. and Ph.D. in Materials Science and Engineering at Carnegie Mellon University. Before joining SNL, he worked for 5 years as a Materials Scientist at the Alcoa research center in Pittsburgh, PA. While at Alcoa, he developed ceramic and metallic materials for operation within the aggressive environments of molten fluoride salt as well as in molten aluminum. The focus of his current research is materials for hydrogen storage. Prior research was focused on the evaluation of materials (alloys, ceramics, and polymers) for use in advanced energy systems.

1.0 Abstract

Efficiencies of greater than 50% in supercritical carbon dioxide (sCO_2) Brayton power cycle systems can be achieved only at turbine inlet temperatures of above 700°C[1]. In support of the push to higher temperatures, a finite element model was developed by Materials Research & Design, Inc. (MR&D) with support from Ceramic Tubular Products, LLC. (CTP) to guide the refinement of CTP's high temperature ceramic multilayer piping. The multilayer technology combines the advantages of a monolithic silicon carbide (SiC) tube and a $SiOC_f$/SiOC ceramic matrix composite (CMC), the result of which is a material with high-temperature strength and stability, high mechanical and thermal shock resistance, and high corrosion resistance. In addition to fabricating test specimens to refine the finite element model, long-duration, high temperature CO_2 exposure tests were performed by Sandia National Laboratories (SNL) on two varieties of inner monolithic SiC.

2.0 Introduction

Among other distinct advantages, sCO_2 cycles have the potential to outperform comparable steam cycles when temperatures ≥450°C are obtained [2]. Up to this point, the majority of materials' research has focused on sCO_2 cycles that would operate at temperatures between 500°C-750°C. At these temperatures, alloys, especially high-nickel alloys such as HAYNES© 230© and INCONEL© 740H©, are being investigated. However, if temperatures up to 700°C and above are to be explored, a new class of materials is needed – advanced ceramics.

In a report issued by the Black and Veatch (B&V) engineering company in 2016, the limitations of the high-nickel alloy, HAYNES© 230©, and other system components were discussed. Under DOE-EERE sponsorship, B&V performed a conceptual design study of a 10 MW_e Concentrating Solar Power (CSP) demonstration plant operating with molten salt and a sCO_2 Brayton cycle energy conversion system [3]. For this study, the turbine inlet conditions were set at 715°C and 25 MPa (3,675 psi) pressure. B&V chose the high-nickel alloy, HAYNES© 230©, for the turbine piping. The report expressed some technical and cost concerns regarding the use of this material which needed to be resolved before a final design was completed for construction and operation. An excerpt from the report states:

> *"The use of HAYNES© 230©, alloy material requires further detailed evaluation in the form of time-dependent creep/fatigue rupture analyses as this is expected to control the design life of the material; hot $sC0_2$ piping design temperatures are in the creep rupture temperature range. Potential cycling temperature, localized stress conditions at supports and other areas should be fully evaluated. The 1,331 °F (721.7 °C) service is a creep rupture consideration and must be further evaluated as creep is expected to be the controlling factor in design."*

In addition to the technical concerns, the wall thickness of the HAYNES© 230© piping needed to meet strength requirements at 720°C had to be set at 5 inches (for 12.5-inch ID piping). This resulted in a cost estimate, for the piping alone, of $20.8M (42%) of the $49.5M total cost estimate for the entire 10 MW_e CSP facility.

The poor high temperature (>700°C) performance and high cost of nickel-based alloys are not the only notable areas of metal piping deficiencies. The corrosion resistance of metal alloys has also been shown to be an area of limitation.

The University of Wisconsin (UW) completed a DOE-NE sponsored NEUP research project (DE-NE0000677) on the corrosion behavior of structural materials for advanced sCO_2 Brayton cycles [4]. Figure 1, extracted from the UW final report, compares the weight change (corrosion) of several structural alloys with SiC after 1,000 hours of exposure to research grade sCO_2 at 750°C. The SiC material was shown to have essentially no weight change, whereas the alloys all showed corrosion-induced weight gains that, if extended through a multiyear lifetime, could severely limit the durability of piping structures made from these alloys. The increase in corrosion rates that is expected for higher operating temperatures of 800-900°C would further limit the durability of metal alloy piping systems.

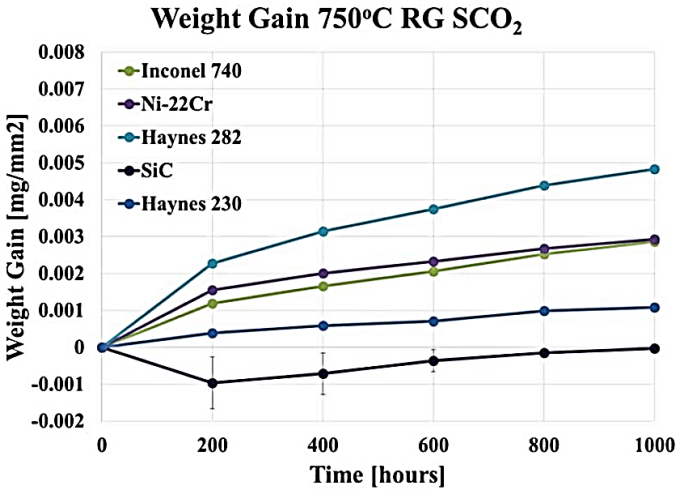

Figure 1. Weight Gain for Austenitic Alloys after Testing in RG sCO_2 at 750°C [4]**.**

These examples along with the DOE's interest in improved $sCO2_2$ Brayton power cycle system components provide the evidence and avenue needed to develop an alternative piping solution with greater high-temperature strength and creep resistance, lower cost, and improved corrosion tolerance.

3.0 Background

Under several DOE sponsored research projects that began in the late 1980's, Gamma Engineering began development of a multilayer tube technology that used advanced ceramic materials for use as accident tolerant fuel (ATF) cladding. The result was a material solution that was able to handle the extreme conditions present in a LOCA (loss-of-coolant accident) in which the fuel clad is exposed to a high level of radiation at temperatures up to an above 1200°C. After more than two decades Gamma Engineering became Ceramic Tubular Products, LLC. (CTP) at which time the technology that had been developed was transferred and adapted for broader applications. Since then, CTP has completed and is currently involved in several DOE sponsored Phase I and Phase II Small Business Innovation Research (SBIR) projects, and commercial projects.

Advanced ceramics have been used in a variety of industries because of their high temperature mechanical strength and high creep resistance, their chemical and atmospheric inertness, and their high wear resistance. Unlike traditional ceramics that are derived from naturally occurring raw materials, advanced ceramics are manufactured using synthetic powders under highly controlled manufacturing processes that result in microstructures that are highly refined [5]. Alumina (Al_2O_3), fused quartz (SiO_2), silicon carbide (SiC), silicon nitride (Si_3N_4), and zirconia (ZrO_2) are a few examples of advanced ceramics [6]. Among these, sintered SiC was chosen as the main material when developing the multilayer technology because of its overall improved material properties, availability at high volumes in large sizes, and price. The properties of monolithic SiC (Hexoloy SE© – Saint-Gobain) are presented in Figure 2.

Maximum Use Temperature	1900°C
Flexural Strength (MPa) @ Room Temp @ 1450°C @ 1600°C	 280 270 300
Density (g/cc)	3.05
Apparent Porosity (%)	5-10
Modulus of Elasticity (GPa) @20°C @1300°C	 420 363
Thermal Conductivity (W/mK) @ 1200°C	34.8
Coefficient of Thermal Expansion	4.02 x 10^-6/°C

Figure 2. Material Properties of SiC Hexoloy SE© [7].

A disadvantage of monolithic SiC and other monolithic advanced ceramics is their brittle nature. When exposed to mechanical and thermal shock loads, monolithic ceramics tend to fail. This characteristic has limited the use of monolithic advanced ceramics in industrial applications. To address this limitation CTP began the development of a multilayer tube technology, known formerly as TRIPLEX, that incorporated a ceramic matrix composite (CMC) around the perimeter of the monolithic SiC, as illustrated in Figure 3. The CMC and/or CMC overwrap consists of multiple micron sized SiC or SiOC (Silicon oxycarbide) fibers and a SiC or SiOC ceramic matrix. SiC CMCs are well known for their excellent creep and thermal shock resistance, low coefficient of thermal expansion, and high temperature properties [8]. The incorporation of the CMC improves the mechanical toughness, thermal shock resistance, and hoop strength of what would otherwise be a bare SiC monolith. Together they provide a material solution that is able to leverage the high temperature properties of both components – the hermeticity and corrosion resistance of the monolithic SiC, and the mechanical and thermal shock resistance of the CMC resulting in a hermetic, temperature stable, corrosion resistant, and tough piping solution.

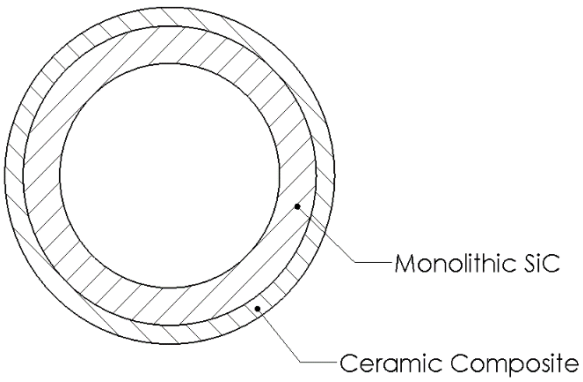

Figure 3. Cross Section of Multilayer Pipe.

Under a recent Solar Energy Technologies Office (SETO) research project, CTP performed thermal shock testing and mechanical shock testing of multilayer tubes (SiC monolith, $SiOC_f$/SiC CMC) of different varieties. The thermal shock tests were performed at Concentrating Solar Technologies Department, Sandia National Laboratories, Albuquerque, NM. The multilayer tube specimens were heated from room temperature up to 900, 1000, or 1100°C before simulated rain (drop diameter of approximately 2-4 mm) was facilitated on the outer surface of the samples. All of the multilayer tube specimens survived the test without fracturing. In previous thermal shock tests, all monolithic specimens fractured when water was applied. Pre-exposed multilayer sample hoop strength results were compared against post-exposed multilayer sample hoop strength revealing that no significant hoop strength reduction occurred. The results of the thermal shock tests are provided in Figure 4.

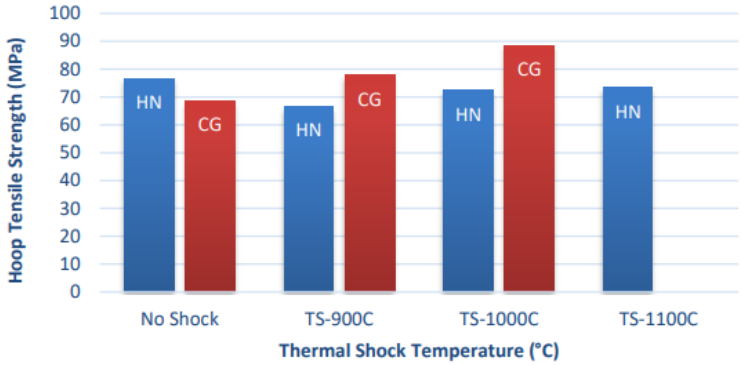

Figure 4. Pre-Exposed and Post-Exposed Thermal Shock Hoop Tensile Strength of Hi-Nicalon (HN) and Nicalon CG (NCG) Multilayer Tube Samples.

Mechanical shock testing of multilayer SiC tubes was performed at MP Machinery and Testing, State College, PA. The test simulated dropping a 12” crescent wrength (1.5 lbs.) on a multilayer SiC tube from a height of 2 feet. In accordance with ASTM E2298, a four-point bend impact test with instrumented striker was used. Certain configurations passed the simulated drop test. The largest contributor to an improved mechanical shock performance was the number of composite layers/plies. The results of the mechanical shock tests are provided in Figure 5.

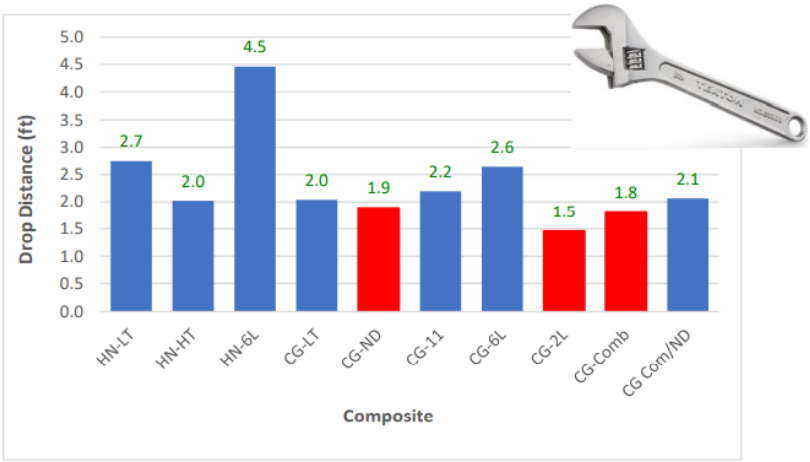

Figure 5. Maximum Survivable Height of Various Multilayer Tube Configurations (HN=Hi-Nicalon fiber, CG=Nicalon-CG fiber, HT= High tension, LT=Low tension, ND= No Debound, L= Layer, 11= 11 fiber wind pattern, Comb=combination fiber wind pattern) from Simulated 2 lb. Crescent Wrench Drop.

To more fully understand the characteristics of the multilayer tube technology and to more efficiently use the constituent advanced ceramic materials and thereby reduce the price of the piping, CTP partnered with Materials Research & Design (MR&D) to evaluate a $SiOC_f$/SiOC CMC with a variety of fiber wind angles, fiber wind tensions, and fiber layers to understand the benefits offered by each. Using in-house, proprietary micromechanics models, MR&D estimated temperature dependent thermal and mechanical properties of the CMC. These micromechanics models were based on well-established composite theory and have been demonstrated for a wide variety of continuous and discontinuous reinforced CMC materials. In support of the model development, CTP first fabricated composite only flat plates. Following the testing of samples taken from the flat plates, CTP fabricated and tested approximately 1-inch diameter multilayer tubes. Once the model was shown to correlate with measured data, the tool was then used to identify peak pressure capabilities and optimized CMC configurations for the final round of larger diameter multilayer tubes that were manufactured and tested by CTP. In addition to developing a finite element model, CTP worked with Sandia National Laboratories (SNL) to validate the monolithic SiC materials' (Hexoloy SE© and Hexoloy SA©) ability to resist corrosion when exposed to high temperature (900°C) CO_2 for durations up to 3000 hours.

4.0 Parametric Finite Element Model

4.1 Finite Element Overview

In the area of composite properties generation for populating the databases, MR&D employed classical micromechanical methods. The mechanical and thermal properties of composite materials are a function of several different parameters, including fiber type, matrix type, fiber volume fraction and layup architecture. Whenever possible, measurements of properties of the type proposed herein should be made so that as many measured properties as possible are available. However, unlike an isotropic material, which has only two (2) independent elastic moduli, one (1) thermal expansion, and one (1) thermal conductivity at any given temperature, composite materials are substantially more complex. If the composite is transversely isotropic, meaning that properties are essentially isotropic in the plane (XY) of the laminate but the properties in the through thickness direction (Z) are different, then at any temperature there are five (5) independent elastic constants, two (2) independent thermal expansions, and two (2) independent thermal conductivities. Orthotropic materials, for which the properties are different in all three orthogonal directions, are even more complex, since there are nine (9) independent elastic properties, three (3) thermal expansions, and three (3) thermal conductivities. This would require numerous measurements to fully characterize the composite material, even if all of these measurements could be made. In addition, it can be difficult to measure all of the Poisson's ratios, even at room temperature, let alone elevated temperatures. Therefore, some other approach, namely micromechanics, must be used in order to determine all of the material property parameters (e.g., stiffness matrix or compliance matrix coefficients, coefficients of thermal expansion, thermal conductivities).

Micromechanics models are constructed based on the known fiber and matrix types and the elastic and thermal properties of these constituents. The models include the volume fractions of these constituent phases, and also include a description of the fiber architecture making up the preform reinforcement, whether it is a tape laminate, a fabric laminate, or a woven/braided preform. The measured composite properties are then used to baseline the micromechanical predictions, so that the known, measured composite properties are reproduced by the micromechanical calculations. The more measured composite properties are available, the better the micromechanical model will be at predicting other properties. When the micromechanical model is able to reproduce all of the available measured

composite properties as well as possible, the remaining output of the model provides the elastic and thermal properties not measured. At the fiber and matrix level, i.e. on the scale of a unidirectional fiber bundle, the micromechanical algorithms used include the composite cylinders assemblage, and the generalized self-consistent scene. At the composite level, classical laminate theory is used for unidirectional/tape laminates of fabric laminates. Volume averages of the stiffness matrix for the fiber/matrix bundles of all of the unique reinforcement directions, transformed to a common global system, are used to calculate the stiffness properties of a multi-directionally reinforced composite.

4.2 Materials Characterization

MR&D began research by determining the constituent property data of the fiber (Nicalon CG) and matrix (SPR-212 preceramic polymer) that CTP validated in the previously, as the material most suitable for the CMC of the multilayer tube for the given application. Both of these materials are considered a silicon oxycarbide (SiOC) as they contain varying volume fractions of beta-silicon carbide, amorphous silicon carbide, amorphous silica, and pyrolytic carbon. The volume fraction of these phases change based on pyrolyzation temperature of the ceramic matrix composite. MR&D assumed a pyrolyzation temperature of 1150°C, which was found in literature [9] to be an optimum processing temperature in regards to stiffness and strength. Initial thermomechanical properties were determined for the phases of beta-silicon carbide (β-SiC), amorphous silicon carbide (a-SiC), amorphous silica (SiO_2), and pyrolytic carbon (PyC). Initial Nicalon CG volume fractions for silicon carbide, silica, and pyrolytic carbon could be determined based upon supplier data regarding the atomic weight and atomic fractions of Si, O, and C. As the pyrolyzation temperature increases for the Nicalon CG fiber, amorphous SiC transforms into β-SiC (α-SiC doesn't start to form until temperatures surpass 1500°C). From a literature review [10] on Nicalon CG pyrolyzation, the volume fractions of the phases for an 1150°C pyrolyzation were determined to be 20% (β-SiC), 34% (a-SiC), 25% (SiO_2), 14% (PyC), and a pore fraction of 7%. Based upon this distribution of volume fractions, the predicted mechanical properties are shown in Table 1.

Table 1. Predicted Properties of Nicalon CG Fiber Pyrolyzed at 1150°C.

Nicalon CG Fiber Properties				
T	E	v	G	p
F	Msi	-	Msi	lbm/in^3
70	26.47	0.204	10.99	0.0921

The SPR-212 preceramic polymer is a methylvinylhydrogen polysiloxane. Shown in Figure 6 is the representative chemical structure of trimethyl terminated vinylmethyl-dimethyl polysiloxane. As shown, there are an 'n' number of methylvinyl siloxanes and an 'm' number of dimethyl siloxanes groups in this polysiloxane chain.

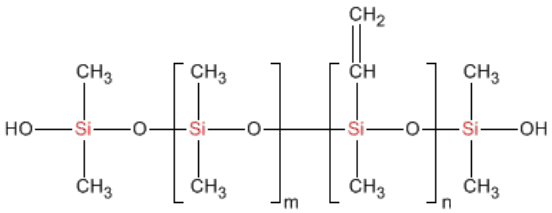

Figure 6. SPR-212 Polymer Chemical Structure.

In order to predict the volume fractions of this preceramic polymer, it was estimated that the polymer chain would produce equal numbers of SiC and SiO_2 compounds with the remainder of the carbons in the vinyl and methyl groups forming PyC. Again, with a pyrolysis temperature of 1150°C, the volume fraction of β-SiC volume fraction compared to a-SiC was cross-checked against literature [9]. The SiOC derived matrix's volume fractions were determined to be 7% (β-SiC), 13% (a-SiC), 42% (SiO_2), 25% (PyC), and a pore fraction of 13%. Based upon this distribution of volume fractions, the predicted mechanical properties are shown in Table 2.

Table 2. Predicted Properties of SiOC Matrix Derived from SPR-212.

SPR-212 SiOC Matrix Properties				
T	E	v	G	p
F	Msi	-	Msi	lbm/in^3
70	10.91	0.206	4.52	0.0759

4.3 Effect of Fiber Wind Angle

After initial mechanical property predictions had been made for the desired CMC layups, MR&D proceeded to predict the mechanical strengths of the CMCs as a function of fiber winding angle. The strength inputs used for this predicted composite strength include a fiber axial strength of 406 ksi, a matrix tensile strength of 11.5 ksi, a matrix compressive strength of 80.8 ksi, and a matrix shear strength of 17.6 ksi. Fiber strength [10] and matrix flexural strength [9] were derived from literature. Shown in Figure 7 is the prediction of hoop strength as a function of fiber wind angle. These predicted strength results match the phenomenological response of a fiber wound pipe according to theory [11]. As the angle moves off the hoop direction, the failure mode transitions from an axial fiber failure to a matrix dominated in-plane shear failure to a matrix dominated transverse failure. Mixed mode failure regions exist between these specified failure modes. As seen in the plot, the hoop strength of the material does see a local peak at 55°. This angle is considered the "ideal" angle for internally pressurized tubes.

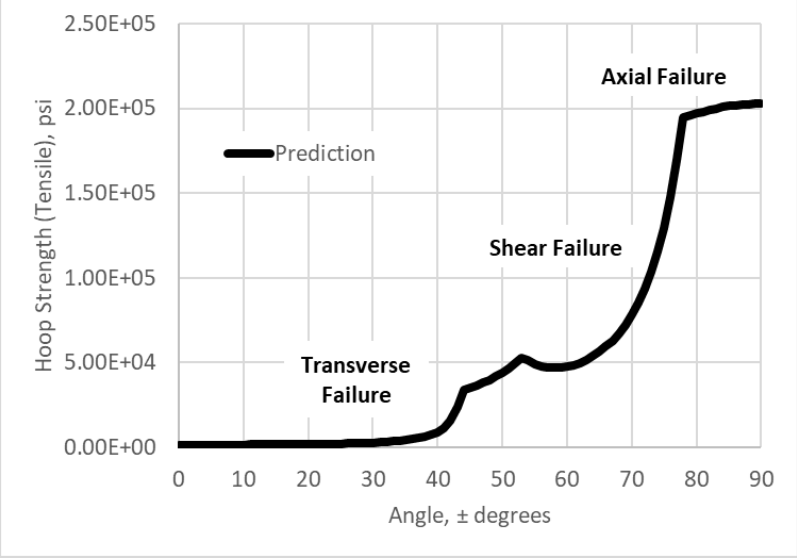

Figure 7. Hoop Strength as a Function of Fiber Wind Angle.

Shown in Figure 8 is the prediction of axial strength as a function of fiber wind angle. This plot is simply the mirror image of the hoop strength plot. As the angle moves off the axial direction, the failure mode transitions from an axial fiber failure to a matrix dominated in-plane shear failure to a matrix dominated transverse failure. For the fiber winding angles that are being investigated, matrix dominated transverse failure will govern the axial strength of any sealed pipe tested. However, if the pipe is free to slide with an O-ring setup, this strength shouldn't govern the pressure containing capabilities of the pipe.

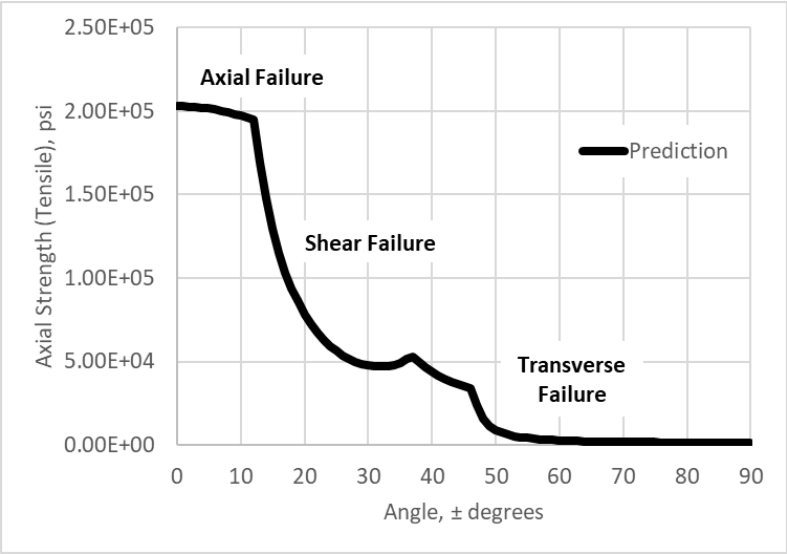

Figure 8. Axial Strength as a Function of Fiber Wind Angle.

Table 3 includes the predicted CMC strengths of a +/− 45° layup, a +/− 54° layup, a 90° (hoop) layup, and a 0°/90° layup. These layups were chosen based on initial discussions with CTP.

Table 3. Predicted CMC Strengths of Specified Layups.

Layup Angle(s)	T11/axial ksi	C11/axial ksi	T22/hoop ksi	C22/hoop ksi	T33/radial ksi	C33/radial ksi	τ12 ksi	τ13 ksi	τ23 ksi
+/- 45	35.20	35.20	35.20	35.20	1.45	10.14	101.55	2.84	2.84
+/- 54	4.71	26.97	51.29	37.22	1.45	9.94	96.60	2.27	3.71
90	1.45	8.30	203.00	337.00	1.45	8.30	17.60	1.45	17.60
0/90	101.55	168.58	101.55	168.58	1.45	10.14	17.60	8.81	8.81

4.4 Residual Stress State of Multilayer Predictions

After establishing a baseline prediction of material mechanical properties and strengths as a function of fiber wind angle, the next task was to determine the stress state of the monolithic SiC pipe as a function of fiber wind angle and fiber tension. For an initial example, a 25 lbf tension was applied to the Nicalon CG wound fibers. The average fiber cross-sectional area per bundle is 0.1216 $mils^2$ which resulted in an axial fiber stress of 206 ksi. With a 50% fiber volume fraction, the effective composite hoop stress of the fiber winding becomes 103 ksi. When taking the angle off the hoop direction into account, 103 ksi is reduced by multiplying it by the $\cos^2$ of the angle. Closed form equations yield a distribution of hoop and radial stress as a function of radial distance for both the monolithic SiC pipe and the CMC.

Shown in Figure 9 is the hoop stress as a function of radial distance for a monolithic SiC pipe with an internal diameter (ID) of 0.75" and an outer diameter (OD) of 1.0". The CMC is wound to an OD of 1.12". Both a hoop wound and a +/− 54° wound pipe are displayed in the figure. The hoop wound CMC puts the monolithic SiC pipe into a hoop compression of ~50 ksi on the ID and ~40 ksi on the OD. Additionally, the +/− 54° wound pipe puts the monolithic SiC pipe into a hoop compression of ~30 ksi on the ID and ~25 ksi on the OD. The values above 0.5" on the plot indicate a hoop stress component experienced by only the Nicalon CG winding fibers. The matrix will not be carrying any of this stress. Property predictions shown in Table 3 will have the axial strength of the Nicalon CG fiber reduced by the winding tension applied.

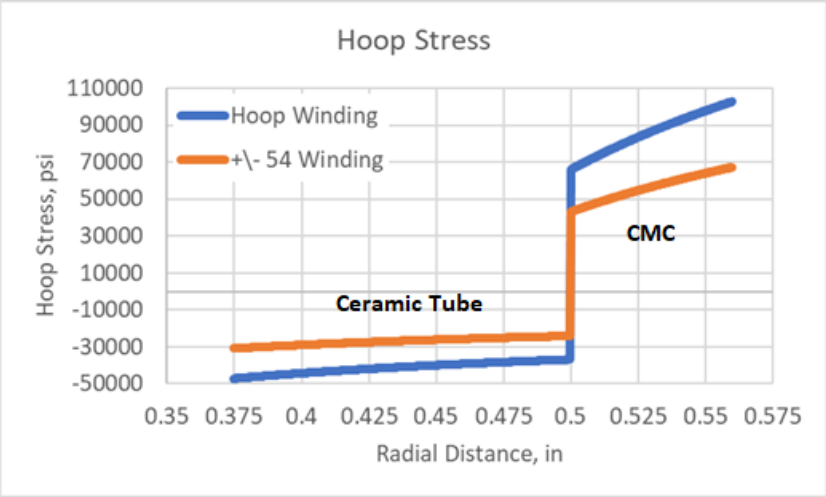

Figure 9. Hoop Stress as a function of Radial Distance.

Shown in Figure 10 is the radial or through thickness stress as a function of radial distance. The stress observed for both winding angles at 0.5" represents the external pressure being applied to the monolithic SiC pipe which puts it into hoop compression. These radial compression stresses shouldn't be a root cause of failure for either material system.

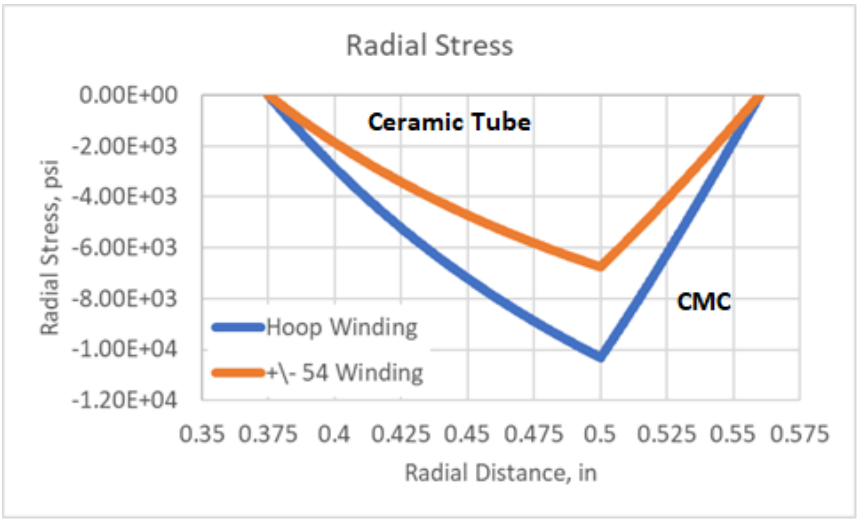

Figure 10. Radial Stress as a function of Radial Distance.

The initial pre-stress in the monolithic SiC can be imported into the ANSYS model before internal pressure is applied. Pre-stress in the CMC was not imported however. As mentioned before, pre-stress in the CMC is only experienced by the Nicalon CG fibers and these fibers have very linear elastic properties. The strength of the CMC will be reduced only in the axial direction as prescribed by the tension load applied to the fibers during winding. However, the mechanical properties will currently remain unchanged.

4.5 ANSYS FEA Model Development

The ANSYS finite element model is able to accommodate changes in monolithic pipe thickness, number of composite layers, winding tension and angle, material properties, as well as thermal and mechanical boundary conditions such as convective heat flux and internal pressure. Shown in Figure 11 is a graphical overview of the ANSYS model considerations.

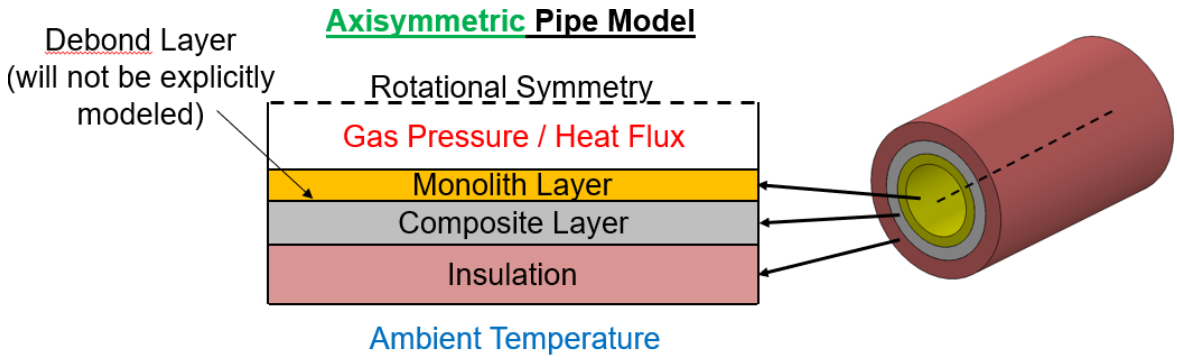

Figure 11. Overview of ANSYS Model Considerations.

Figure 12 shows and example of how various wind angles can be evaluated throughout the composite stack-up by changing inputs in the ANSYS APDL code. As previously mentioned, predicted properties for a wide variety of wind angles are available to the simulation so that any composite stack-up can be analyzed.

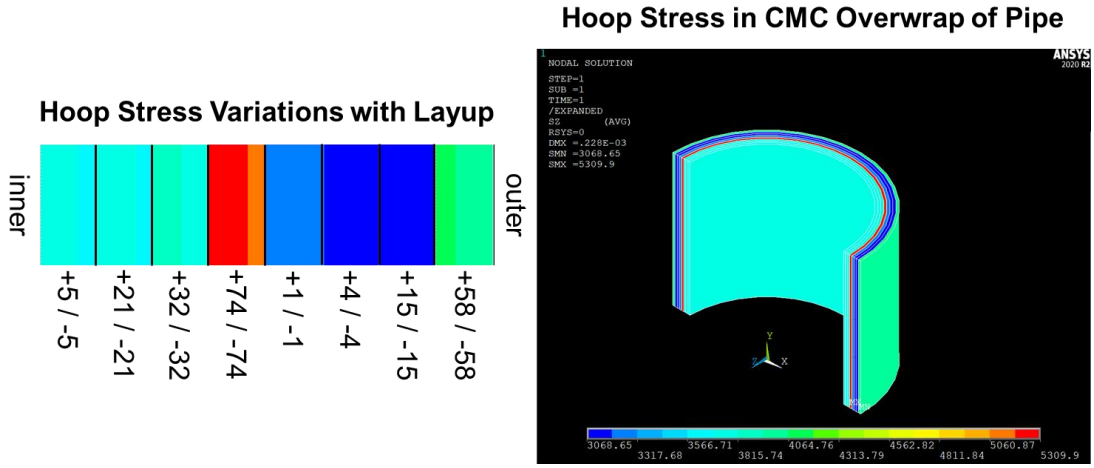

Figure 12. Example Composite Stack-Up in Finite Element Model.

4.6 ANSYS Finite Element Simulation Overview

MR&D began the development of a parametric ANSYS FEA tool with the analysis of a composite cylinder under representative heat and pressure loads given a set of user inputs. A lengthwise axisymmetric representation of the composite cylinder pipe was determined to be the most useful and computationally effective for this parametric model. The model was designed to give the user the ability to specify radial geometry parameters including (1) SiC monolith inner radius, (2) SiC monolith thickness, (3) composite ply number and ply thickness (CMC layer thickness), and (4) insulation thickness. Additionally, the length of the pipe can be defined as well for heat transfer problems as the temperature of the pipe and the sCO_2 are axially dependent.

As an initial demonstration, MR&D set the inner radius to 1-inch, the SiC monolith thickness to 0.25-inch, the ply number to five (5) with a single ply thickness of 0.2-inch, and the insulation thickness to 0.25-inch. Figure 13 shows the axisymmetric pipe of the composite cylinder within ANSYS. The coordinate system for the analysis was set so that the X-axis is the radial direction, the Y-axis is the axial direction, and the Z-axis is the circumferential direction. Effective properties for each of the three components (monolithic SiC, $SiOC_f$-SiOC composite, and insulation) are prescribed by the user.

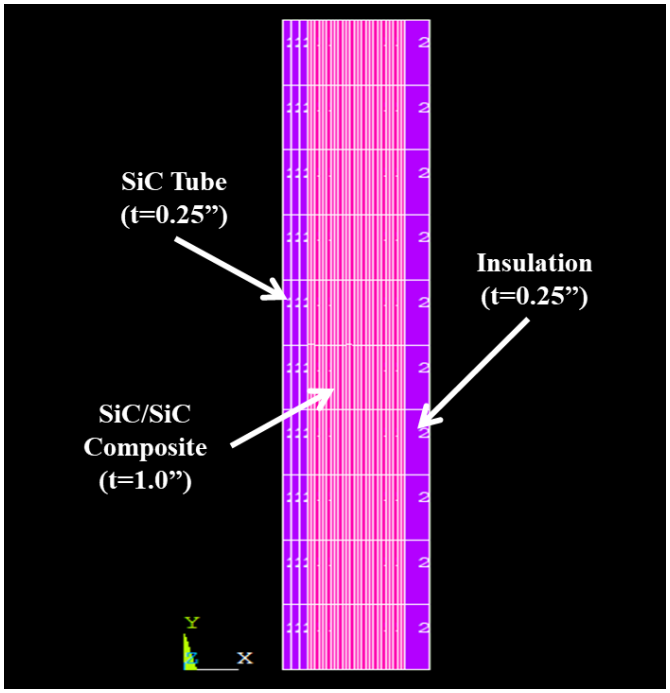

Figure 13. Axisymmetric Pipe for Analysis of Composite Cylinder under Heat and Pressure Loads.

In addition to geometric and material property input considerations, boundary conditions are able to be prescribed and these include: (1) inlet pressure, (2) inlet temperature (3) inlet mass flow rate, (4) outer ambient temperature, and (5) initial stress state from manufacturing. Inlet pressure is used to determine the mechanical loading on the pipe as well as the correct properties of the sCO_2. Inlet temperature is used to determine the correct temperature dependent properties of the sCO_2 as well as for heat transfer calculations. Inlet mass flow rate is used for heat transfer calculations. Outer ambient temperature is used for both external radiation and natural convection. The initial stress state from manufacturing can be fed into the model by defining the fiber tension, fiber wind angle, and fiber volume fraction.

4.7 Structural Finite Element Model

In order to evaluate the coupled effect that the initial stress state from manufacturing and the inner pressure have on the multilayer pipe, a stress analysis was performed in ANSYS, as shown in Figure 14. The pipe was fixed along the bottom edge in the Y (axial) direction. Additionally, the top nodes were coupled in the Y (axial) direction so they expanded uniformly to the same extent.

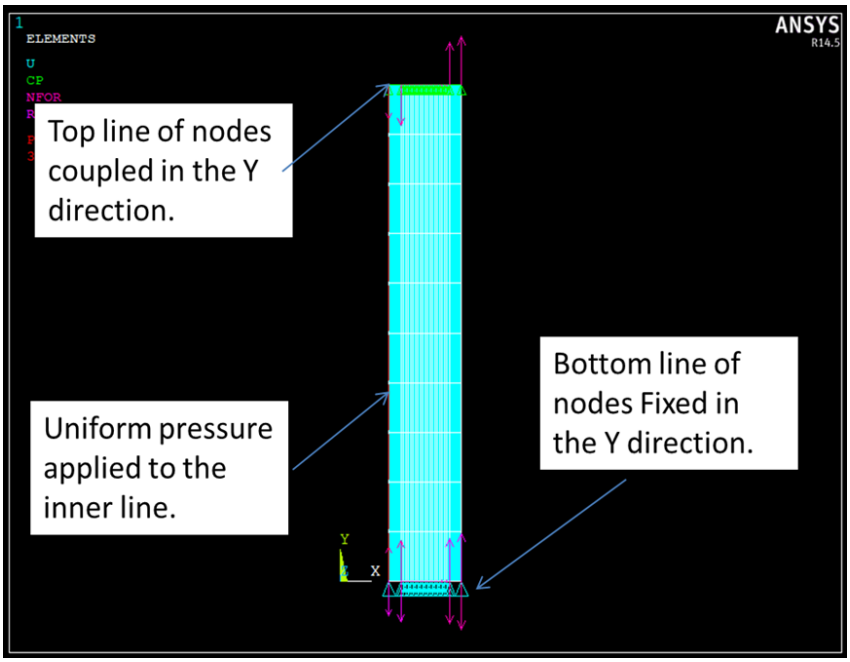

Figure 14. Boundary Conditions for Structural Analysis of Composite Cylinder.

The initial stress from manufacturing was applied using the *INISTATE* command to apply the closed form solutions in a CSV table array format, which allowed ANSYS to use the centroid of each element to linearly interpolate the correct stress value to be applied to each element.

Figure 15 shows the stress results of the applied initial stress state from manufacturing with the inner pressure applied. The top images of Figure 15 shows the radial stress and the bottom image of Figure 15 shows the hoop stress of the monolithic SiC, $SiOC_f$-SiOC CMC, and insulation. In these models, the insulation is merely 'going along for the ride' as it has minimal stiffness contribution and no initial stress from manufacturing. The radial stress of the entire pipe is under a compressive stress. For hoop stress, the monolithic SiC is under hoop compression while the CMC is under varying amount of hoop tension. The axial stress is negligible as assuming free expansion in the radial direction.

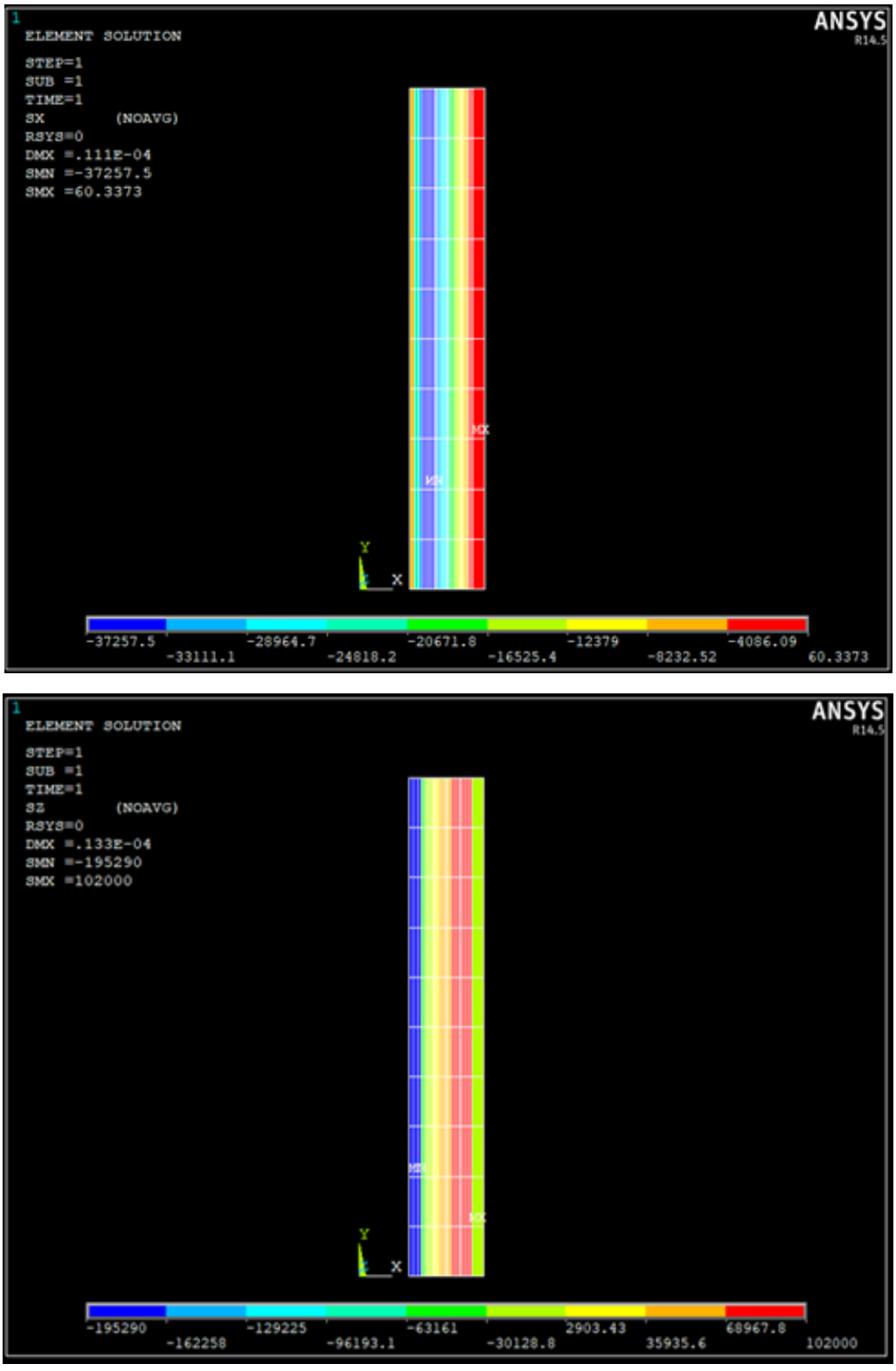

Figure 15. Structural Analysis Results. Top – Radial Stress. Bottom – Hoop Stress.

4.8 Material Property and Strength Updates

CTP provided MR&D with flat, composite plate data that was measured by Westmoreland Mechanical Testing & Research, Inc (WMT&R) to correlate the material properties performances with the model's predictions. Tensile, compressive, and thermal conductivity samples were taken from the flat plates.

CTP partnered with Lancer Systems to fabricate the three (3) $SiOC_f/SiOC$ composite only flat plates. These plates were composed of four (4) plies of Nicalon CG 8HS fabricate sheets approximately 19.0" x 7.0" coated with a multilayer PyC/SiC interface coating. The interface coated sheets were stacked and then infiltrated with Starfire System's SPR-212 slurry precursor, followed by lamination and curing in an autoclave. The cured plates were then densified using the SPR-212 precursor and nine (9) polymer infiltration and pyrolysis (PIP) cycles by Lancer Systems. A pyrolysis temperature of 1000°C was used for these plates. CTP preferred that a pyrolysis temperature of 1150°C, as a lower processing temperature would not correlate with the research that MR&D had performed. However, Lancer Systems was limited by a max furnace temperature of 1000°C. The resulting thicknesses of the flat plates are shown in Table 4. One of the completed flat plates is presented in Figure 16.

Table 4. Composite Flat Plate Thicknesses.

Plate	Min Thickness (in.)	Max Thickness (in.)	Average Thickness (in.)
1	0.099	0.107	0.103
2	0.094	0.111	0.103
3	0.087	0.099	0.093

Figure 16. Densified $SiOC_f/SiOC$ Composite Plate.

All of the flat plates underwent ultrasonic testing (UT) at Physical Sciences Incorporated (PSI) before being machined into test specimens. The UT scan reported the density of the panel related to the speed of sound in the material. If a delamination was found, the signal intensity would go to zero. All of the panels tested at PSI were uniform with minimal void space.

4.8.1 Test Specimens

4.8.1.1 Tensile Test Specimen

With guidance from ASTM C1275-18 "Standard Test Method for Monotonic Tensile Behavior of Continuous Fiber-Reinforced Advanced Ceramics with Solid Rectangular Cross-Section Test Specimens at Ambient Temperature", CTP chose to use an edge-loaded flat specimen geometry. Test specimens were cut from the flat composite plates by PSI using a laser cutter. The specimen geometry and a specimen are shown in Figure 17.

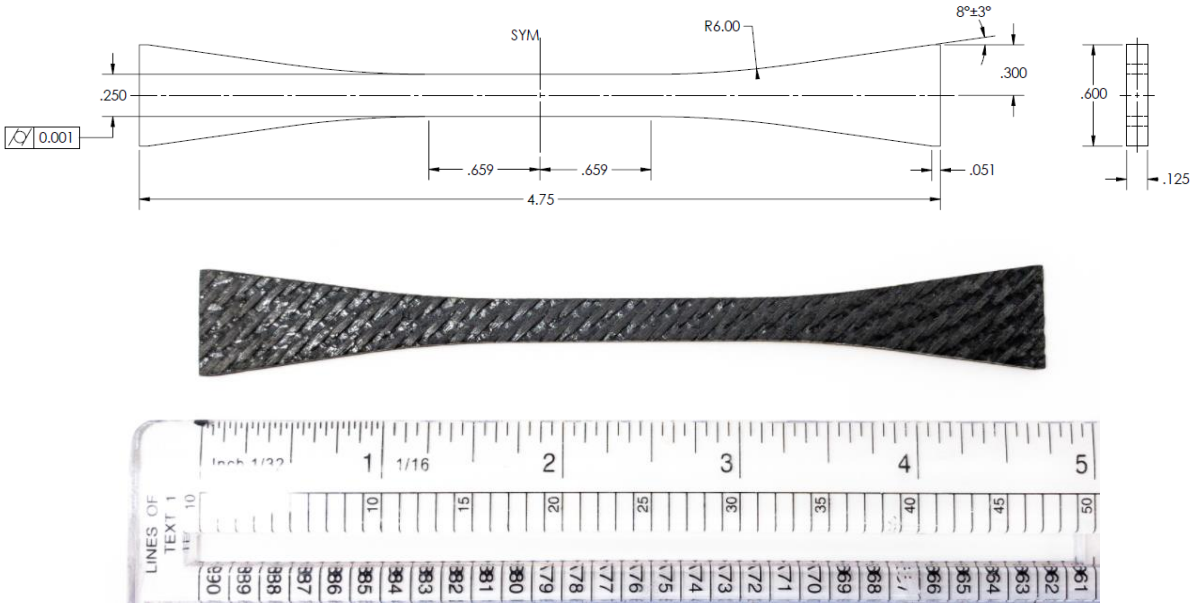

Figure 17. Tensile Test Specimen Geometry/Dimensions (top) and Specimen (bottom).

Specimens were cut at both a 0°/90° and a 45°/45° fiber orientations, as shown in Figure 18, to better validate the results of the micromechanical model.

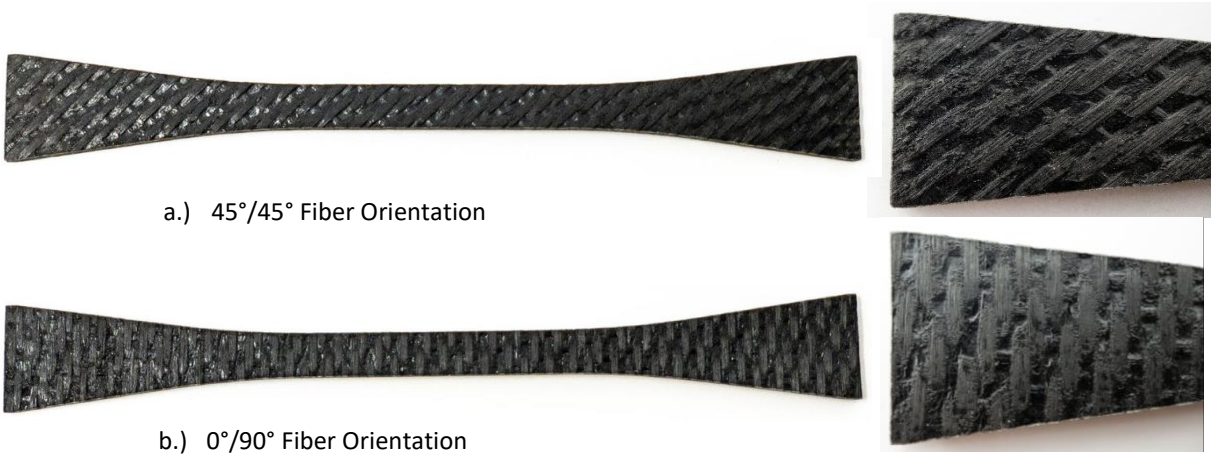

a.) 45°/45° Fiber Orientation

b.) 0°/90° Fiber Orientation

Figure 18. Tensile Test Specimen with 0°/90° and 45°/45° Fiber Orientations.

4.8.1.2 Compression Test Specimen

The geometry for the compression test specimens was chosen with guidance from ASTM C1358-18 "Standard Test Method for Monotonic Compressive Strength Testing of Continuous Fiber-Reinforced Advanced Ceramics with Solid Rectangular Cross Section Test Specimens at Ambient Temperatures". Test specimens were cut from the flat composite plates by PSI using a laser cutter. The compression test specimen geometry and a specimen are shown in Figure 19.

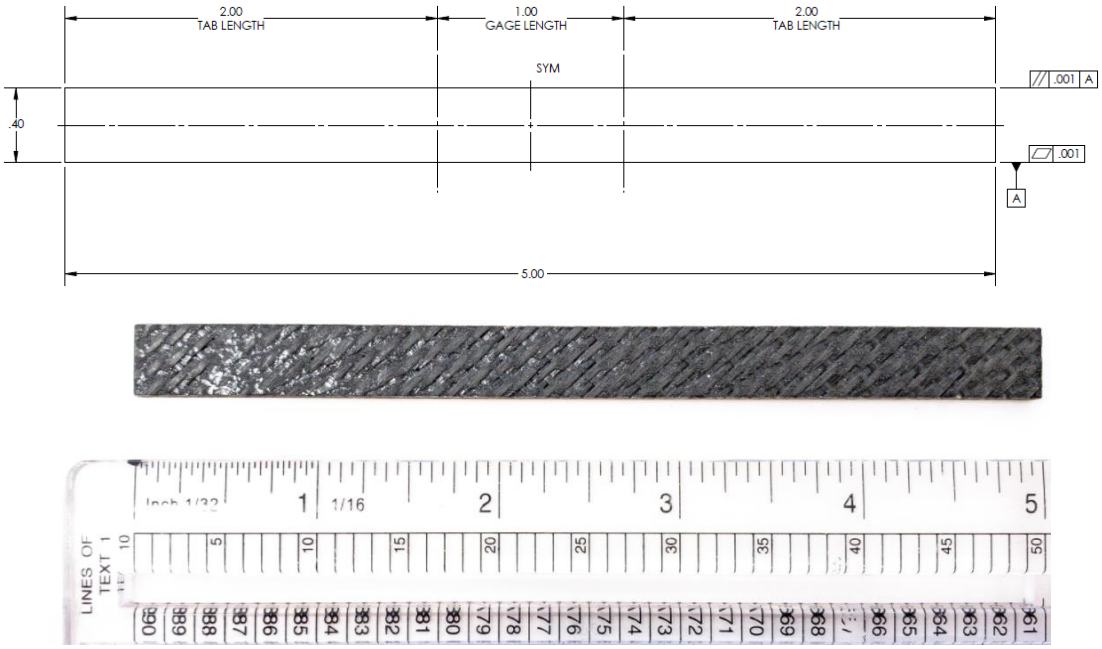

Figure 19. Compression Test Specimen Geometry/Dimensions (top) and Specimen (bottom).

As was performed on the tensile test specimens, the compression specimens were cut at both a 0°/90° and a 45°/45° fiber orientations, as shown in Figure 20, to better validate the results of the micromechanical model.

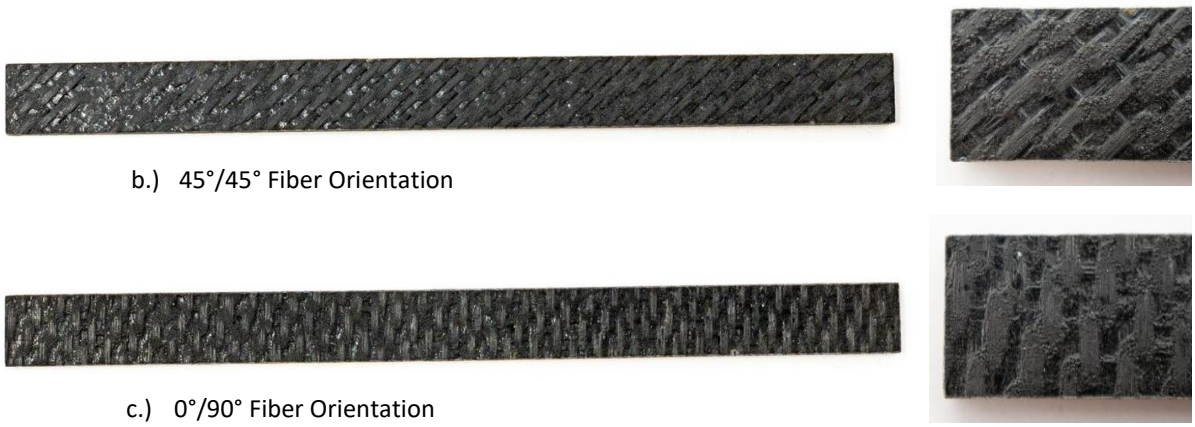

b.) 45°/45° Fiber Orientation

c.) 0°/90° Fiber Orientation

Figure 20. Compression Test Specimen with 0°/90° and 45°/45° Fiber Orientations.

4.8.1.3 Thermal Conductivity Test Specimen

The geometry for the thermal conductivity test specimens was chosen with guidance from ASTM E1461, "Standard Test Method for Thermal Diffusivity by the Laser Flash Method". Test specimens were cut from the flat composite plates by PSI using a laser cutter. A thermal conductivity specimen is shown in Figure 21.

Figure 21. Thermal Conductivity Specimen (0.5" Diameter).

Prior to testing, room temperature density measurements were performed for each of the specimen. Each plate was then tested at 600, 800, and 1000°C using a TA instruments DFL1200 laser flash system. The results of the testing are shown in Table 5.

Table 5. Thermal Conductivity Test Results.

Specimen ID	Density (Bulk)	Temperature	Diffusivity	Specific Heat	Conductivity
	[g/cc]	[°C]	[cm^2/s]	[J/g*K]	[W/m*K]
TC-18	2.235	600	0.0100	1.29	2.88
		800	0.0097	1.39	3.01
		1000	0.0098	1.39	3.04
TC-19	2.235	600	0.0101	1.25	2.82
		800	0.0102	1.33	3.03
		1000	0.0100	1.30	2.91
Average	2.235	600	0.0101	1.27	2.85
		800	0.0100	1.36	3.02
		1000	0.0099	1.35	2.98

Table 6 shows a comparison of the measured room temperature modulus and in-plane tensile strength with predictions made by MR&D that were previously shown in Table 3.

Table 6. Comparison of Measured and Predicted Modulus and Strength for Two Layup Directions.

Layup	Measured Modulus	Predicted Modulus	Measured Strength	Predicted Strength
0/90	11.6 MSI	**13.6 MSI**	19.3 ksi	**101.5 ksi**
+45/-45	11.1 MSI	**13.1 MSI**	9.8 ksi	**35.2 ksi**

A comparison of the values shown in Table 6 shows that MR&D's predictions were higher than what was measured. After confirming the processing steps, fiber volume fraction and seeing photos of the failed specimens, MR&D looked in literature to find the reason for the poor strengths. They discovered that the tensile strength of Nicalon CG fiber decreases significantly with long exposure times, as shown in Figure 22. Also considering the process to coat the fibers, which is applied at 1180°C, the Nicalon CG fibers were subjected to multiple thermal cycles that could affect the integrity of the fiber.

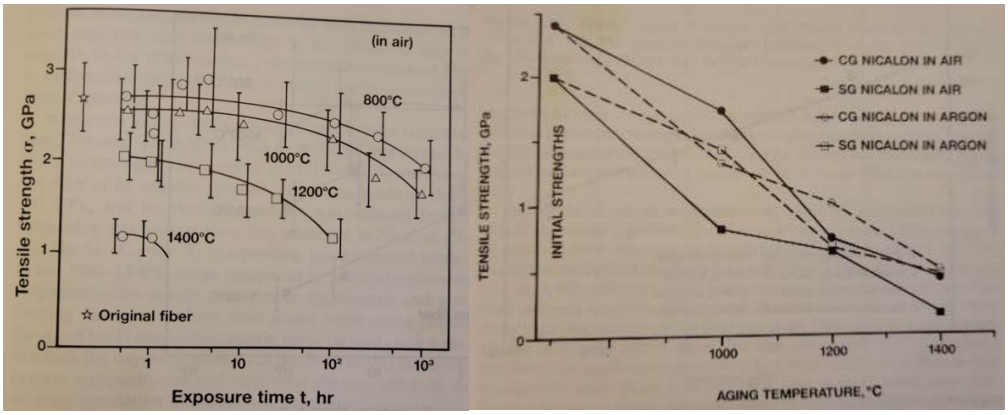

Figure 22. Decreasing Strength of Nicalon CG Fiber as a Function of Exposure Time (left) and Temperature (right) [10].

Figure 23 also shows one of the stress-strain curves that was measured by WMT&R. Clearly the material exhibited a nonlinear response after a "yield" stress was reached. However, MR&D's initial models assumed a linear elastic behavior for the CMC. For this purpose, and since failure in the CMC is not expected before failure in the ceramic, MR&D modified the elastic properties of the fiber to match the measured composite properties shown in Table 6. In addition to modifying the fiber elastic properties, MR&D also found that a fiber volume fraction of 35% (instead of 50%) was also beneficial for correlation. While this is a number that could change based on ply thickness and wind angle, the value was fixed for the material property predictions. Once the stiffness was correlated, MR&D used the reduced fiber properties to predict properties for wind angles ranging from +/-0° through +/- 90° in 1° increments. Table 7 shows a summary of the elastic properties for a variety of wind angles.

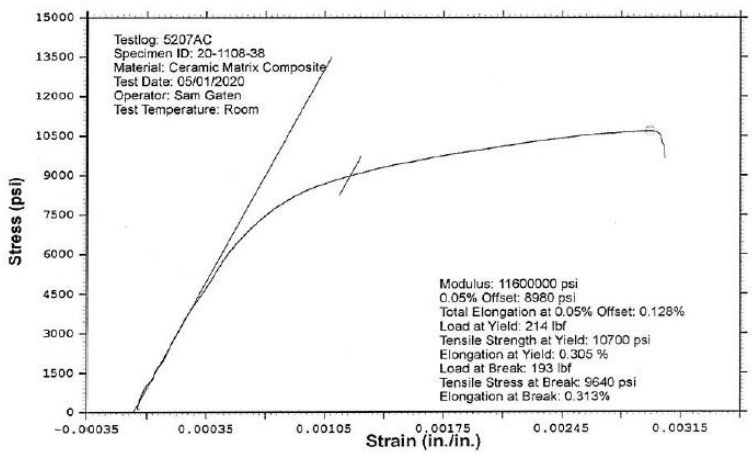

Figure 23. Stress vs. Strain Curve for Tensile Specimen (+45/-45).

Table 7. Updated Elastic Properties for Various +/- Wind Angles.

Wind Angle	E_x (Thru-Thickness)	E_y (Axial)	E_z (Hoop)	ν_{xy}	ν_{xz}	ν_{yz}	G_{xy}	G_{xz}	G_{yz}
	(MSI)	(MSI)	(MSI)				(MSI)	(MSI)	(MSI)
+0/-0	9.15	14.52	9.15	0.1977	0.4272	0.3134	3.9	3.2	3.9
+15/-15	9.2	13.8	9.2	0.206	0.412	0.327	3.9	3.3	4.2
+30/-30	9.3	12.2	9.6	0.238	0.367	0.345	3.79	3.4	4.6
+45/-45	9.4	10.58	10.58	0.299	0.299	0.325	3.59	3.59	4.78
+60/-60	9.33	9.6	12.2	0.367	0.238	0.271	3.4	3.79	4.59
+75/-75	9.2	9.23	13.83	0.412	0.206	0.219	3.26	3.93	4.19
+90/-90	9.16	9.16	14.5	0.4272	0.1977	0.1976	3.21	3.99	3.99

4.9 Preliminary Tube Test and Model Correlation

CTP provided MR&D with preliminary pipe test results that included both SiC monolith and multilayer sample results. The multilayer tubes were fabricated using two (2) different monolith wall thicknesses and three (3) different CMC thicknesses that incorporated either 2, 4, or 6 fiber layers. A debond layer was applied to some of the inner monolithic SiC tubes. The pipes were tested according to the conditions outlined under ASTM C1819-15 – "Standard Test Method for Hoop Tensile Strength of Continuous Fiber-Reinforced Advanced ceramic Composite Tubular Test Specimens at Ambient Temperature Using Elastomeric Inserts".

All tests were performed using an Instron model number 5982. A diagram of the hoop test is shown in Figure 24, along with a multilayer specimen prepared for test.

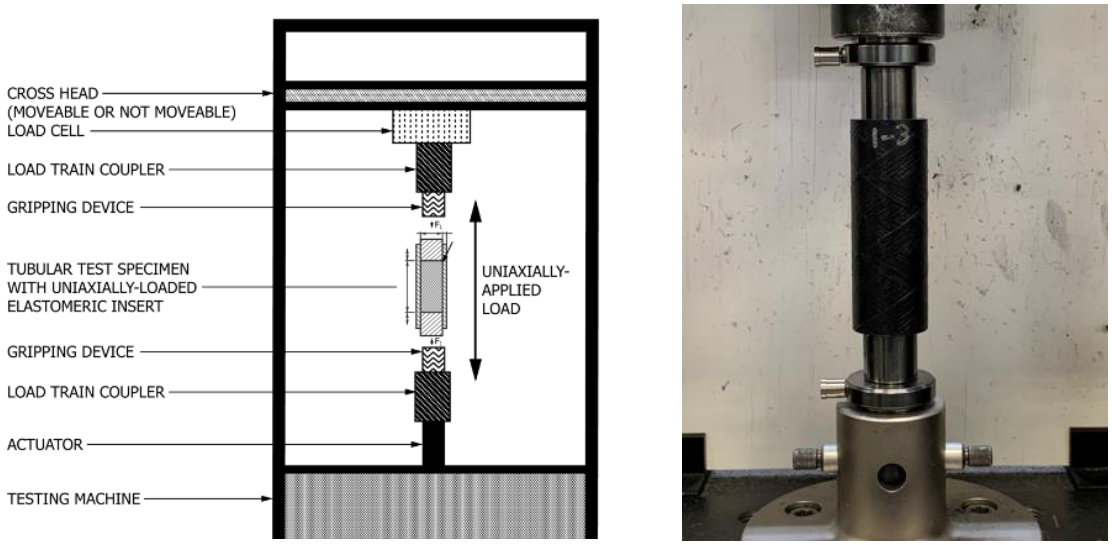

Figure 24. Diagram of Hoop Test Setup (ASTM C1819-15) (left), Multilayer Specimen Prepared for Hoop Test (right).

The multilayer tube has three (3) important radius points, r_0, r_1, r_2, as shown in Figure 25. The inner radius of the monolith and the entire tube is, r_0. This is the location of the maximum hoop stress during the failure of the monolith. The contact radius between the monolith outer surface and the composite layer inner surface is, r_1.This is the location of the maximum hoop stress during the composite failure. The final radius is the outer radius of the entire multilayer tube, r_2

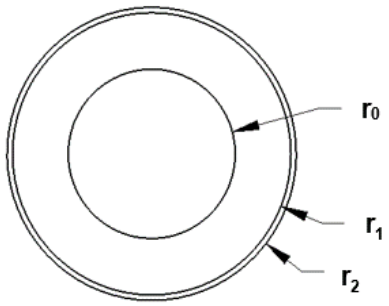

Figure 25. Multilayer Tube Specimen Geometry.

CTP manufactured 26 multilayer tubes. The tubes contained an inner Hexoloy SE SiC monolithic tube that was surrounded by an $SiOC_f$/SiOC CMC of one of three specified thicknesses. 14 of the 28 tubes had an inner diameter (ID) of 0.75”, an outer diameter (OD) of 1.0”, and a length of 27.0” (100 series). 7 of these 14 tubes had a debond layer applied to the inner monolithic SiC tube. 12 of the 28 tubes had an inner diameter (ID) of 0.75”, an outer diameter (OD) of 1.25”, and a length of 27.0” (125 series). 6 of these 12 tubes had a debond layer applied to the inner monolithic SiC tube. The Nicalon CG fiber was filament wound onto the SiC monoliths using CTP’s two-axis filament winder. After winding, a PyC/SiC interface coating was applied to the fiber. The interface coated tubes were then PIPed by Starfire Systems using their SPR-212 slurry precursor at a pyrolysis temperature of 1000°C. After receiving the completed tubes, CTP sectioned them into appropriately sized hoop test specimens. Table 8 outlines the various multilayer specimen configurations produced. An example of a 100X4 and 125X4 specimen is presented in Figure 26.

Table 8. Tube Sample Matrix with Dimensions – Multilayer 1-inch OD Tubes.

Specimen	Layers	Debond Layer	# of Samples	Specimen Length (in.)	Avg. r_0 (in.)	Avg. r_1 (in.)	Avg. r_2 (in.)	Avg. CMC thickness (in.)
100X2	2	No	3	3.125	0.366	0.499	0.532	0.033
100D2		Yes	5		0.366	0.500	0.535	0.035
100X4	4	No	5	3.375	0.366	0.499	0.564	0.065
100D4		Yes	5		0.365	0.499	0.558	0.059
100X6	6	No	5	3.625	0.366	0.501	0.589	0.088
100D6		Yes	5		0.368	0.503	0.586	0.083
125D2	2	Yes	5	4.125	0.366	0.627	0.665	0.038
125X4	4	No	4	4.375	0.365	0.628	0.701	0.073
125D4		Yes	5		0.365	0.626	0.699	0.073
125X6	6	No	8	4.625	0.366	0.629	0.733	0.103
125D6		Yes	5		0.366	0.630	0.731	0.101

Figure 26. Top-down View of 100X4 and 125X4 Specimen (left) and Specimen Cross-section (right).

The monolith only specimens were obtained from a monolithic Hexoloy SE SiC tube from Saint-Gobain. CTP sectioned the tube into appropriate lengths for hoop testing. Table 9 outlines the dimensions of the monoliths tested.

Table 9. 0.56" OD Monolithic SiC Sample Measurements.

Sample	r_0 (in.)	r_1 (in.)	Sample Length (in.)
1	0.215	0.279	1.564
2	0.215	0.279	1.557
3	0.212	0.277	1.550
4	0.212	0.278	1.584
5	0.213	0.279	1.573
Average	0.213	0.278	1.565
SD	0.002	0.001	0.013
Max	0.215	0.279	1.584
Min	0.212	0.277	1.550

The results from the initial hoop testing on SiC multilayer and monolithic samples are shown in Table 10 and Table 11, respectively. Figure 27 compares the maximum hoop stress of the various tube configurations with each other. An average hoop stress of 27,388 psi was obtained from the five (5) monolithic samples tested. Considering the published flexural strength is 40 ksi, MR&D believed the 27 ksi value to be reasonable.

Table 10. Hoop Test Results – Multilayer 1-inch OD Samples.

Specimen	Debond Layer	# of Samples	Specimen Length (in.)	Test Rate (in./min)	Max Pressure (psi)	Max Pressure Std Dev. (psi)	Max Hoop Stress (psi)
100X2	No	3	3.125	0.25	9081	615	30307
100D2	Yes	5		0.25	8710	528	28890
100X4	No	5	3.375	0.25	8670	545	28867
100D4	Yes	5		0.25	9984	374	32955
100X6	No	5	3.625	0.25	9294	897	30644
100D6	Yes	5		0.25	9376	619	30924
125D2	Yes	5	4.125	0.25	15316	323	31098
125X4	No	4	4.375	0.25	14619	590	29502
125D4	Yes	5		0.25	16164	379	32788
125X6	No	8	4.625	0.25	15781	571	31887
125D6	Yes	5		0.25	15793	1401	31902

Table 11. Hoop Test Results – 0.56" OD Monolithic SiC Samples.

Sample	Sample Length (in.)	Test Rate (in./min)	Max Load (lbf)	Max Pressure (psi)	Max Hoop Stress (psi)
1	1.564	0.25	1,208.90	8,325	32,603
2	1.557	0.25	1,139.30	7,882	30,709
3	1.550	0.25	845.6	5,989	22,852
4	1.584	0.25	948.7	6,719	25,427
5	1.573	0.25	952.6	6,715	25,349
Average	1.565		1,019.00	7,126	27,388
Std Dev.	0.013		150	953	4,087

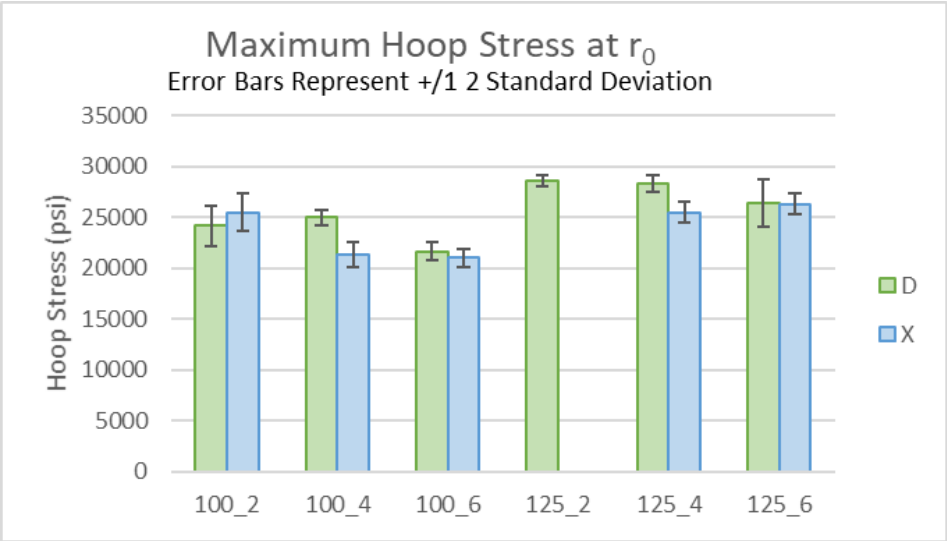

Figure 27. Maximum Hoop Stress of Multilayer 1-inch OD Specimens.

Using a ceramic strength of 27.3 ksi, MR&D revisited the finite element model and analyzed the multilayer variations to correlate with the measured failure pressures. Figure 28 shows a plot of maximum hoop stress in the ceramic for a monolithic pipe (orange) line and a multilayer pipe with three different wind tension values (0 lbf, 0.292 lbf and 10 lbf). 0.292 lbf of pre-tension was applied during the manufacturing. 0 lbf and 10 lbf were also included to provide lower and upper bounds. The results suggest that an increased pressure of 9,342 psi would be required to generate a 27.3 ksi hoop stress on the ID of the multilayer pipe.

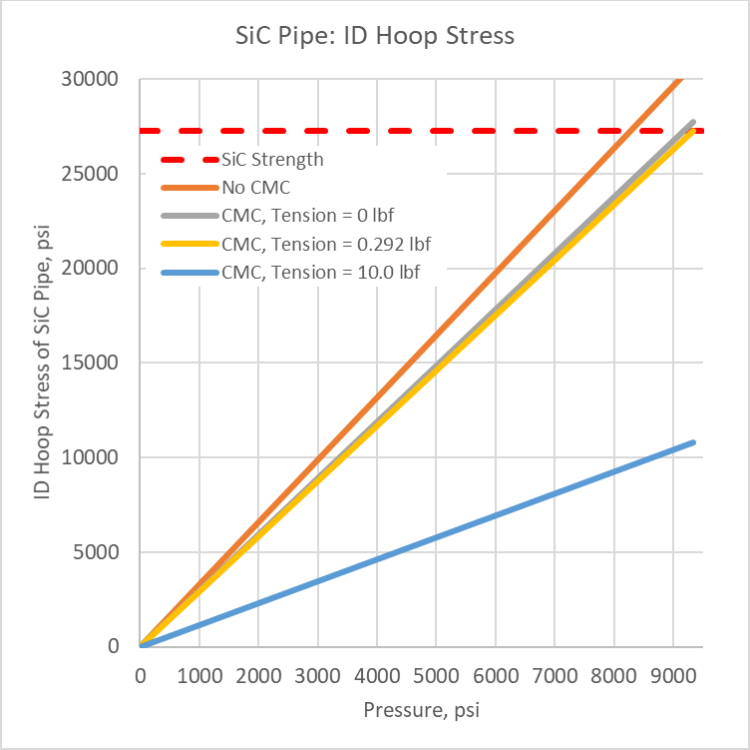

Figure 28. Preliminary Hoop Wrap Tension Parametric Study.

Figure 27 shows the results of the multilayer pipes where the average failure pressure of the thinner walled multilayer tubes was measured to be 9,186 psi across all variants and the thicker walled multilayer tubes was measured to be 15,535 psi across all variants. This resulted in a higher peak hoop stress in the ceramic than MR&D predicted. At this stage, MR&D believed that the low failure pressure prediction (9,342 psi) was due to the estimated properties for the composite material. However, as will be discussed later, it appeared that the low prediction was due to an underestimation of the SiC monolith strength.

Using the model, MR&D determined the load sharing between the monolith and the CMC. In preparing for this study, MR&D evaluated the residual strength of the wound CMC. Using the updated CMC properties for a +55/-55 wound composite, Figure 29 shows how the residual hoop strength decreases with increasing wind tension. For this estimation, only the strength of the fiber is affected by the winding tension as the matrix is applied after winding has completed. The results show that at around 10 lbf, the fiber is no longer stronger than the matrix.

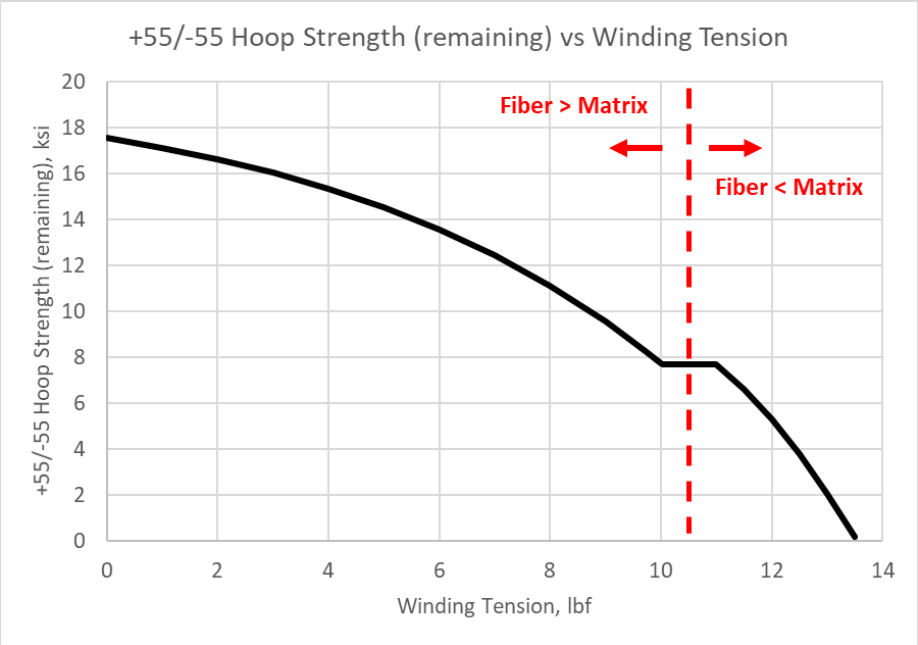

Figure 29. Estimated Residual Strength of +55/-55 Wound CMC.

Building on these results MR&D generated a carpet plot which summarized how the model predicted the relationship between failure pressure, SiC pipe thickness, and fiber pretension, as shown in Figure 30. For the design space (i.e., expected SiC pipe dimensions), the thickness of the SiC monolith had the largest influence on increasing the failure pressure. However, the number of plies or fiber layers of the CMC and the winding tension did additionally increase the failure pressure, especially with thinner wall SiC pipes. Additionally, from these simulations, the CMC was never predicted to fail first. Also shown in this plot are red dots which represent samples from the initial test series. Note that these samples were all wound with low fiber tension so they mostly show the trend of SiC monolith thickness and failure pressure.

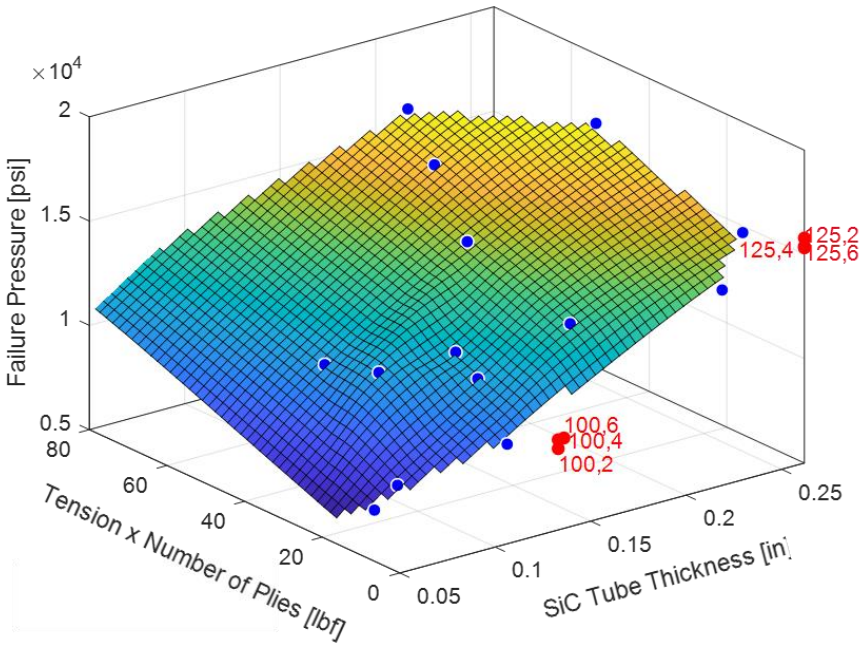

Figure 30. MR&D Predicted Relationship between Failure Pressure, SiC Tube Thickness and Ply Tension.

After receiving available tube sizes from St. Gobain, CTP asked MR&D to use the developed model to estimate what thickness CMC overwrap would be required to achieve a 6100 psi failure pressure given a 1.5" OD tube with a 1.0" ID (0.25" wall thickness) wrapped with a CMC with either a pure +/-54° or a pure +/-90° overwrap. Using the model, MR&D determined that on its own, the monolith was capable of surviving a 6100 psi internal pressure without any CMC. While a CMC overwrap could be capable of increasing the pressure limit of the tube, the thickness and/or wind tension were beyond what CTP was capable of producing at that time. In order to maximize the number of specimens which could be fabricated, CTP set four (4) fiber layers as the limit. Since a 0.25" thick tube would not be significantly affected by four (4) layers of composite overwrap, MR&D's focus shifted to determining what ceramic wall thickness would be required for the four-layer overwrap to be able to significantly increase the pressure load capabilities of the SiC tube.

Since 1.5" OD x 1.0" ID tubes were already acquired, the 1.5" outer radius was held constant. In MR&D's simulations, the ID design space would start at 1.0" and increase up to 1.4". The goal was to find the tube thickness which would be required for four (4) layers of +55°/-55° overwrap (layer thickness = 0.01733") to increase the pressure capability of the multilayer tube. Figure 31 shows the results from this design and analysis trade study. In this plot, the pipe thickness is on the vertical axis with the winding tension on the horizontal axis. The colors in the contour represent a stress/strength ratio where values above 1.0 show failure in the ceramic. The results show that the multilayer tube would fail once the thickness is below 0.12". The minimum thickness is further reduced if additional tension could be applied to the fiber. However, > 3 lbf of tension would be required and manufacturing methods at that time did not allow for such a load.

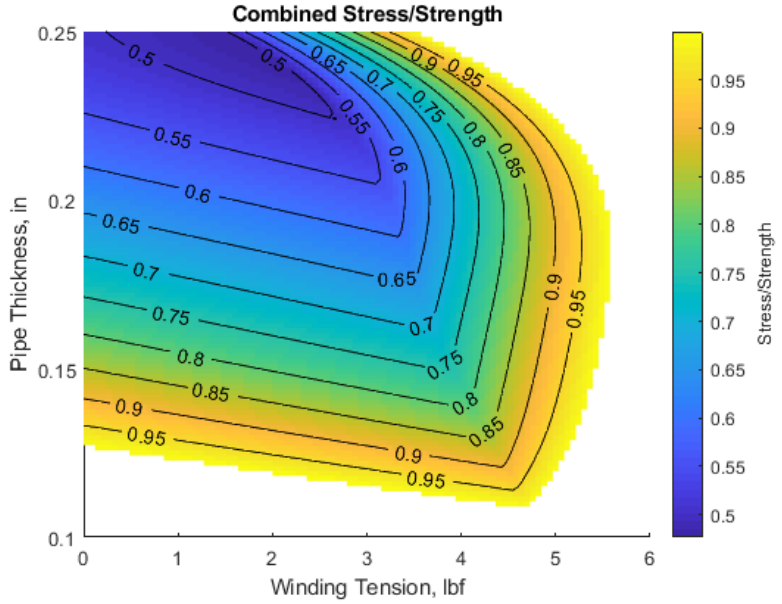

Figure 31. Design Space for Ceramic Tube with Four Layers of +55/-55 Overwrap (CMC).

After conversing with St. Gobain, it was determined that thinner-wall tubes could not be acquired leaving the best available option to OD grind the current 1.5” OD x 1.0” ID tubes. Thus, MR&D revised the design trade study to fix the ID at 1.0” while decreasing the OD of the tube from 1.5” down to 1.1”. All other assumptions previously described were made. Figure 32 shows the updated results from this design and analysis trade study. The results show that the multilayer ceramic tube would fail once the thickness is below 0.10”. Once again, the minimum thickness could be further reduced if additional tension could be applied to the fiber. However, the concern then became how to grind the SiC monolith to such a small thickness.

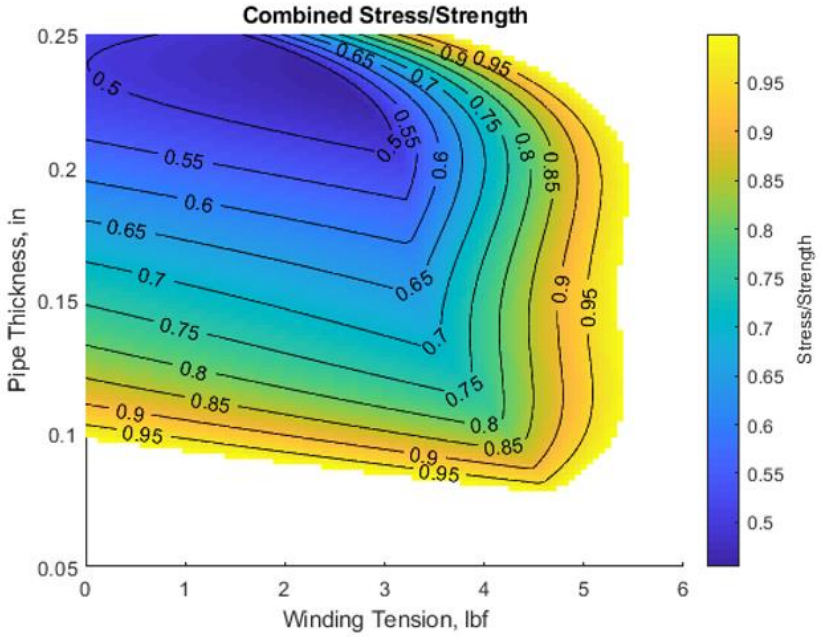

Figure 32. Updated Design Space for SiC Monolith with Four Layers of +55/-55 Overwrap (CMC).

After reviewing the model's predictions, it was decided that the 1.5" OD tubes would be sent out for machining to achieve a wall thickness of 0.1". Following discussions with the machine shop, it was decided that 0.1" was too thin for the wall thickness so the value was changed to 0.125". Table 12 shows the updated samples that were chosen for fabrication. Tubes 12 & 13 were composite only tubes (no inner ceramic tube) which were included to help MR&D correlate with predicted composite properties. Two (2) monolithic tube configurations with no CMC were also included, one with the original 1.5" OD and a second which was ground down to 1.25".

Table 12. Tube Sample Matrix – Multilayer and Monolithic 1.25-inch OD Tubes, Multilayer and Monolithic 1.50-inch OD Tubes.

Configuration	Description	Notes on FEA
125NCG-4X21L	1.25" OD Monolith, Nicalon CG, 4 Layers, +/-55° Architecture, 2:1 Wind Pattern, 1 lb Tension	**2 FEA cases (with and without pre-stress)**
125NCG-4H21L	1.25" OD Monolith, Nicalon CG, 4 Layers, +/-87° Architecture (Hoop Wind), 2:1 Wind Pattern, 1 lb Tension	**1 FEA case (with pre-stress)**
125NCG-4C21L	1.25" OD Monolith, Nicalon CG, 4 Layers, Combined Architecture ((+/-55°, Hoop (87°), Hoop (87°), 55°)), 2:1 Wind Pattern, 1 lb Tension	*Mixed angle design; not analyzed.*
125NCG-4X11L	1.25" OD Monolith, Nicalon CG, 4 Layers, +/-55° Architecture, 1:1 Wind Pattern, 1 lb Tension	*Same as Tubes 1 and 2 for FEA purposes*
125NCG-4X81L	1.25" OD Monolith, Nicalon CG, 4 Layers, +/-55° Architecture, 8:1 Wind Pattern, 1 lb Tension	*Same as Tubes 1 and 2 for FEA purposes*
125NCG-4X21H	1.25" OD Monolith, Nicalon CG, 4 Layers, +/-55° Architecture, 2:1 Wind Pattern, High Tension (3 lb)	**1 FEA case (with pre-strss)**
125NCG-4X21L-ND	1.25" OD Monolith, Nicalon CG, 4 Layers, +/-55° Architecture, 2:1 Wind Pattern, 1 lb Tension, No De-Bond Coating	*Same as Tubes 1 and 2 for FEA purposes*
125NCG-4X21L-COMP	1.25" OD Monolith, Nicalon CG, 4 Layers, +/-55° Architecture, 2:1 Wind Pattern, 1 lb Tension, Composite Only	**2 FEA cases (with and without pre-stress)**
150NCG-4X21L	1.50" OD Monolith, Nicalon CG, 4 Layers, +/-55° Architecture, 2:1 Wind Pattern, 1 lb Tension	**1 FEA case (with pre-stress)**
150HEXOLOY	1.50" OD Monolith Only	**1 FEA case (without pre-stress)**
125HEXOLOY	1.25" OD Monolith Only	**1 FEA case (without pre-stress)**

Specifically, CTP manufactured 15 multilayer tubes. 13 of the 15 multilayer tubes contained an inner Hexoloy SE SiC monolithic tube that was surrounded by an $SiOC_f$/SiOC CMC. 2 of the 15 multilayer tubes contained an inner graphite mandrel that was surrounded by an $SiOC_f$/SiOC CMC. In a later step, these 2 tubes had the inner graphite mandrel removed, which left the composite on its own. 13 of the 15 multilayer tubes including the tubes with a graphite mandrel had an inner ID of 1.0", an outer OD of 1.25", and a length of 24.0". 2 of the 15 multilayer tubes had an ID of 1.0", an OD of 1.50", and a length of 24". The Nicalon CG fiber was filament wound onto the mandrels using CTP's four-axis filament winder that was acquired in the later part of the project. After winding, a PyC/SiC interface coating was applied to the fiber. The interface coated tubes were then PIPed by Starfire Systems using their SPR-212 slurry precursor at a pyrolysis temperature of 1000°C. After receiving the completed tubes, Herb's Tool sectioned them into appropriately sized hoop test specimens. Table 13 outlines the various multilayer and monolithic test samples that were produced. The processed, full-length multilayer tubes are shown in Figure 33. Several of the hoop test samples are presented in Figure 34.

Table 13. Sample Dimensions – Multilayer and Monolithic 1.25-inch OD Tubes, Multilayer and Monolithic 1.50-inch OD Tubes.

Configuration	# of Samples	Specimen Length (in.)	Avg. r_0 (in.)	Avg. r_1 (in.)	Avg. r_2 (in.)	Avg. CMC thickness (in.)
125NCG-4X21L	5	3.60	0.495	0.626	0.690	0.064
125NCG-4H21L	7	3.60	0.494	0.626	0.686	0.060
125NCG-4C21L	7	3.60	0.496	0.626	0.687	0.061
125NCG-4X11L	3	3.60	0.498	0.626	0.687	0.061
125NCG-4X81L	3	3.60	0.490	0.626	0.689	0.064
125NCG-4X11L/4X18L	6	3.60	0.494	0.626	0.688	0.062
125NCG-4X21H	7	3.60	0.496	0.626	0.678	0.052
125NCG-4X21L-ND	7	3.60	0.494	0.626	0.687	0.062
125NCG-4X21L-COMP	7	2.12	0.625	0.625	0.689	0.064
150NCG-4X21L	3	4.72	0.494	0.755	0.819	0.064
150HEXOLOY	1	4.32	0.492	0.753	NA	NA
125HEXOLOY	2	3.06	0.492	0.626	NA	NA

Figure 33. Fully Processed Multilayer Tubes.

Figure 34. Top-down View of 125 HEXOLOY, 125NCG-4X21L, 150 HEXOLOY, and 150NCG-4X21L Hoop Test Samples – Left to Right (top left), Specimen Cross-section of 125 Multilayer Hoop Test Samples (top right), Top-down View of All Multilayer Hoop Test Sample Configurations – 125NCG-4X21L, 125NCG-4H21L, 125NCG-4C21L, 125NCG-4X11L, 125NCG-4X81L, 125NCG-4X21H, 125NCG-4X21L-ND – Left to Right (bottom).

4.10 Tube Pre-Test Predictions

Following a review of the test matrix, MR&D ran ten (10) finite element simulations which served as pre-test predictions for the 1.25" multilayer, 1.25" monolith, 1.5" multilayer, and 1.5" monolith specimens. These ten (10) simulations are identified in the last column of Table 12. For this round, MR&D did not independently analyze the 2:1 and 8:1 wind pattern nor did they independently analyze specimens with and without a debond coating. For the case of the wind pattern, the composite is currently modeled as a homogenized material. Since prior simulations do not show composite failure before ceramic failure, MR&D did not feel it was necessary to include an explicit definition of the unit cell size in the axisymmetric model. In regard to the debond layer, additional test data, such as double cantilever or end-notch flexure, would be required to generate an accurate representation of the bondline. Thus, MR&D performed one simulation for the cases with and without a de-bond layer.

All of these simulations were performed using the multi-step process previously described where the prestress in the SiC monolith and CMC overwrap were calculated using closed-form theory and defined in the model as an initial stress state. MR&D applied an internal pressure of 6100 psi as part of a second load case. Since the stress response is linear with pressure, MR&D was able to scale the stresses in the ceramic to determine the failure pressure. Lastly, an assumed strength of 27.3 ksi was used for the ceramic based on the initial monolithic results. While preliminary 1-inch multilayer tube tests showed that the ceramic was failing at a stress just over 30 ksi, MR&D decided to keep using the 27.3 ksi strength because it was a strength that was directly measured in a test of a monolithic tube. Figure 35 provides a summary of the simulations.

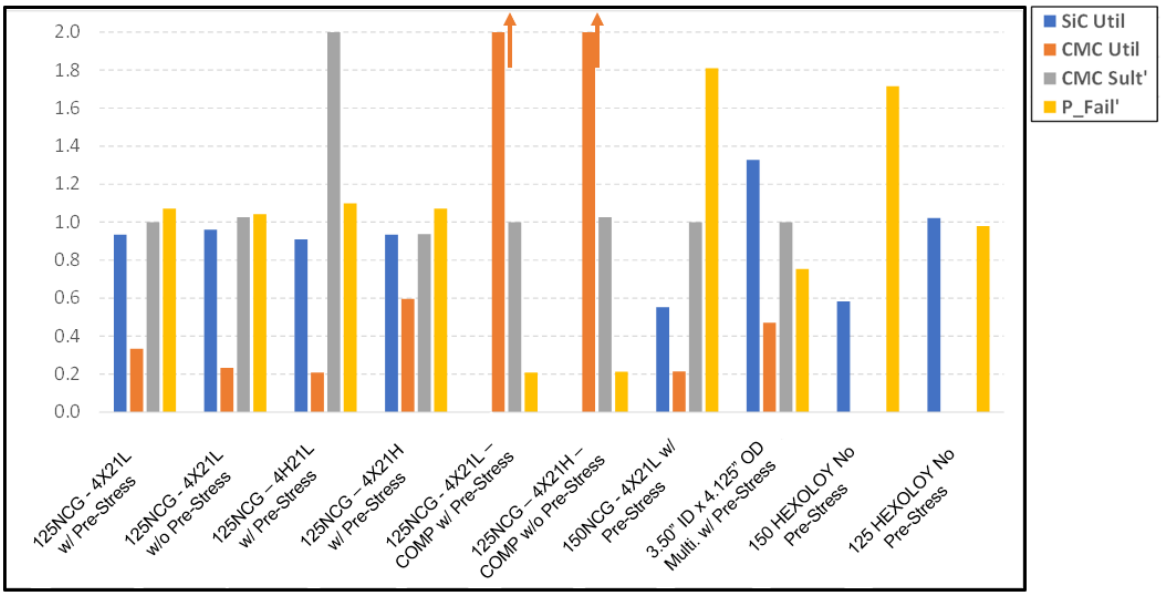

$$SiC\ Util = \frac{SiC\ SZ_{Max}}{27.2\ ksi} \qquad CMC\ Util = \frac{CMC\ SZ_{Max}}{CMC\ SZ_{Ult}} \qquad CMC\ Sult' = \frac{CMC\ SZ_{Ult}}{CMC\ SZ_{Ult,2-1}} \qquad P\_Fail' = \frac{P\_Fail}{6100\ psi}$$

Figure 35. Summary of Multilayer and Monolithic 1.25-inch OD Specimens, Multilayer and Monolithic 1.50-inch OD Specimens Simulations.

In short, for a given SiC tube size (ID+OD), adding the CMC overwrap offered a slight reduction in SiC hoop stress, or equivalently, a slight increase in the expected failure pressure. This conclusion is consistent with the findings that were generated on previous test results and pre-test predictions. The SiC monolith has a higher utilization (i.e., stress-to-strength ratio) and its dimensions are the primary parameters that control the failure pressure. Among the four (4) cases for multilayer tubes with diameters of 1.00", 1.25" and 1.346", the SiC utilization fell in a relatively narrow range of 0.91 to 0.96. This result shows that the fiber tension and fiber angle had a very minor impact on the stress in the tubes that were tested. This is once again another finding that was consistent with previous simulations. While the different wind angles affected the strength and stiffness of the composite, none significantly affected the measured failure pressure of the multilayer tube. When using a multialyer SiC tube of 1.0" ID, 1.5" OD instead of 1.0", 1.25", the SiC utilization (or stress) was significantly reduced, from 0.93 (2-1) to 0.55 (2-8). Also, the multilayer SiC tube of 1.0", 1.5" provided a slightly lower SiC utilization relative to the monolithic design (0.55 vs. 0.58, 2-8 vs. 2-9).

Table 14 summarizes the predicted failure pressures for the test specimens. As previously mentioned, MR&D did not independently evaluate the 1:1 and 1:8 wind patterns or the variation without a debond layer.

Table 14. Predicted Failure Pressure of Multilayer and Monolithic 1.25-inch OD Specimens, Multilayer and Monolithic 1.50-inch OD Specimens.

Configuration	Description	Monolith ID and OD (in.)	MR&D Predicted P_{max1} (psi)
125NCG-4X21L	Standard Wind	1.0" ID, 1.25" OD	6533
125NCG-4H21L	Circumferential Wind	1.0" ID, 1.25" OD	6706
125NCG-4C21L	Combined Wind	1.0" ID, 1.25" OD	
125NCG-4X11L	1/1 Wind Pattern	1.0" ID, 1.25" OD	
125NCG-4X81L	1/8 Wind Pattern	1.0" ID, 1.25" OD	
125NCG-4X11L/4X18L	1/1 & 1/8 Wind Patterns	1.0" ID, 1.25" OD	
125NCG-4X21H	High Tension Standard Wind	1.0" ID, 1.25" OD	6919
125NCG-4X21L-ND	No-Debond Standard Wind	1.0" ID, 1.25" OD	
125NCG-4X21L-COMP	Composite Only Standard Wind	NA	1270
150NCG-4X21L	Standard Wind - Increased Wall Thickness	1.0" ID, 1.5" OD	11042
150HEXOLOY	Monolith Only - Increased Wall Thickness	1.0" ID, 1.5" OD	10466
125HEXOLOY	Monolith Only	1.0" ID, 1.25" OD	5973

4.11 Final Tube Test Correlation

After testing the samples, CTP sent MR&D the test data. Without details on strain or displacement, the only parameter with which the model could correlate with was the failure pressure. The last three columns in Table 15 show the measured failure pressure, predicted failure pressure, and percent difference.

Table 15. Predicted Failure Pressure Compared to Tested Failure Pressure of Multilayer and Monolithic 1.25-inch OD Specimens, Multilayer and Monolithic 1.50-inch OD Specimens.

Configuration	Description	Monolith ID and OD (in.)	Measured P_{max1} (psi) - Average	MR&D Predicted P_{max1} (psi)	% Difference
125NCG-4X21L	Standard Wind	1.0" ID, 1.25" OD	7154	6533	-8.68%
125NCG-4H21L	Circumferential Wind	1.0" ID, 1.25" OD	6936	6706	-3.32%
125NCG-4C21L	Combined Wind	1.0" ID, 1.25" OD	7158		
125NCG-4X11L	1/1 Wind Pattern	1.0" ID, 1.25" OD	7112		
125NCG-4X81L	1/8 Wind Pattern	1.0" ID, 1.25" OD	6649		
125NCG-4X11L/4X18L	1/1 & 1/8 Wind Patterns	1.0" ID, 1.25" OD	6881		
125NCG-4X21H	High Tension Standard Wind	1.0" ID, 1.25" OD	7139	6919	-3.08%
125NCG-4X21L-ND	No-Debond Standard Wind	1.0" ID, 1.25" OD	6381		
125NCG-4X21L-COMP	Composite Only Standard Wind	NA	1457	1270	-12.85%
150NCG-4X21L	Standard Wind - Increased Wall Thickness	1.0" ID, 1.5" OD	12371	11042	-10.74%
150HEXOLOY	Monolith Only - Increased Wall Thickness	1.0" ID, 1.5" OD	7978	10466	31.18%
125HEXOLOY	Monolith Only	1.0" ID, 1.25" OD	6799	5973	-12.15%

As seen in Table 15, MR&D consistently underpredicted the failure pressure of the multilayer tube. Originally, the expectation was that MR&D would overpredict the failure pressure since the finite model element model is ideal and flawless where the actual specimens would likely contain microflaws and cracks which could serve as failure initiation points. However, after looking over the correlation more closely, MR&D believed that the failure pressure underprediction was due to the assumption that the ceramic would fail when the hoop stress at the ID exceeded 27.3 ksi. If you consider the 1.0” ID/1.25” OD specimens in Table 15, each failed at an average hoop stress of 30 ksi. This average hoop stress is slightly lower than the hoop stress on the previous set of multilayer hoop tests. The previous 0.75” ID/1.0” OD specimens had an average hoop stress of 30.4 ksi. Additionally, the 0.75” ID/ 1.25” OD specimens had an average hoop stress of 31.4 ksi. Table 16 shows what the updated failure pressure predictions if MR&D used 30.97 ksi as the failure strength of the ceramic. With this update, MR&D slightly overpredicted the failure pressures in the majority of the specimens. This is more in line with what was originally expected. The major outlier was the 1.0” ID, 1.5” OD specimen which had a nearly 50% error. It is important to note that this is data point was taken using only three (3) samples. MR&D and CTP believed that something unexpected happened such as a major defect in the monolithic SiC tube. CTP is currently working on developing NDE techniques to ensure material correctness. Lastly, the 12.85% difference for the composite only specimen is more that acceptable for a model of this type. However, following a review of the correlation effort, MR&D was able to discuss the differences in how the composite was processed in both tube and flat plate form with CTP. As previously mentioned, MR&D estimated composite properties based on flat plate data, shown previously in Table 7. While the fiber, interface coating, matrix and PIP cycles were the same for both, the tubes were produced via filament winding while the plates used 2D fabric. The filament winding process has the ability to produce very uniform and dense structures, thus the fiber volume fraction of the wound tubes is likely greater than the 35% value MR&D calculated form the flat plate data. As an increase in fiber volume fraction would increase the strength of the composite and, thus, the failure pressure for the composite only simulation.

Table 16. Updated Predicted Failure Pressure of Multilayer and Monolithic 1.25-inch OD Specimens, Multilayer and Monolithic 1.50-inch OD Specimens.

Description	Monolith ID and OD (in.)	Measured P_{max1} (psi) - Average	MR&D Predicted P_{max1} (psi)	% Difference
Standard Wind	1.0" ID, 1.25" OD	7154	7235	1.13%
Circumferential Wind	1.0" ID, 1.25" OD	6936	7633	10.05%
Combined Wind	1.0" ID, 1.25" OD	7158		
1/1 Wind Pattern	1.0" ID, 1.25" OD	7112		
1/8 Wind Pattern	1.0" ID, 1.25" OD	6649		
1/1 & 1/8 Wind Patterns	1.0" ID, 1.25" OD	6881		
High Tension Standard Wind	1.0" ID, 1.25" OD	7139	7436	4.16%
No-Debond Standard Wind	1.0" ID, 1.25" OD	6381		
Composite Only Standard Wind	NA	1457	1270	-12.85%
Standard Wind - Increased Wall Thickness	1.0" ID, 1.5" OD	12371	12569	1.60%
Monolith Only - Increased Wall Thickness	1.0" ID, 1.5" OD	7978	11913	49.32%
Monolith Only	1.0" ID, 1.25" OD	6799	6799	-0.01%

Both the model's predictions and the tests performed proved that the maximum hoop stress and the resulting failure pressure of the multilayer tubes were not heavily affected by a variation in the parameters used to manufacture the CMC. The multilayer tubes that were fabricated using the standard wind performed as well or better than all other variations. Multilayer tubes fabricated using the combined wind, 1/1 wind pattern, and high tension had similar performance when compared to tubes using the standard wind. The configuration that performed worst was the 1/8 wind pattern (11% decrease when compared to the standard wind). This decrease in performance may have been a result of the increased fiber cross-over points.

Although the primary or initial failure (monolith only) of the multilayer tube was not heavily impacted by a variation in the CMC configuration, the final failure (monolith and composite) was largely impacted by the wind type. Figure 36 compares the failure loads of the monolith (initial failure) with the failure loads of the CMC and monolith (final failure). In almost every case, the CMC failed after monolithic failure.

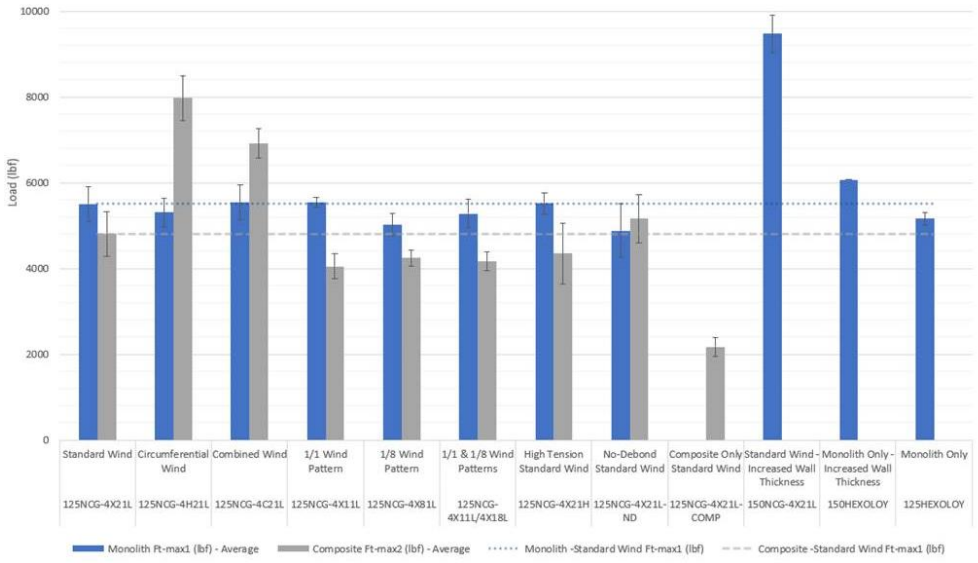

Figure 36. Failure loads of Monolith vs. Composite (After Monolith Failure).

The load carrying capacity at the final failure was heavily influence by the wind type especially in the case of a helical wind (standard, 1/1, 1/8, and High Tension), circumferential wind (hoop), and combined wind (helical and circumferential). The circumferential wind configuration provided, on average, a 69% increase in load carrying capacity over the helical wind. The combined wind configuration provided, on average, a 46% increase in load carrying capacity over the helical wind. Additionally, the way in which the multilayer tubes fail at the final failure was heavily influence by the wind type. This was in large part because certain configurations were able to hold higher loads/pressures and therefore released much more energy at the time of failure. A photo of failed specimen from the helical (standard), circumferential, and combined wind configurations is shown in Figure 37.

Figure 37. Failed Multilayer 1.25-inch OD Hoop Specimens 125NCG-4X21L (Helical/Standard Wind), 125NCG-4H21L (Circumferential/Hoop), and 125NCG-4C21L (Combined) – Left to Right.

At failure the multilayer tube samples fabricated using a helical (standard) wind remained the most intact. At failure, the CMC remained largely intact with a thin crack running down the length of the tube and stopping before either end. The multilayer tube samples fabricated using a circumferential wind failed catastrophically leaving, in most cases, a whole section of the tube missing. The multilayer tube samples fabricated using a combined wind failed in a similar manner as the tubes fabricated using a standard wind with a much greater release of energy at the time of composite failure.

4.12 Large Tube Predictions

After updating the model with the revised material properties, MR&D was directed to identify a ceramic tube wall thickness and CMC thickness for three (3) new test cases defined below. The test cases were based on "real-world" sCO_2 Brayton cycle pipe sizes and operating pressures.

- 1.77" ID, Max P 6,200 psi, Room temp and 900°C, FoS of 1 and 2 – Based upon correspondence with sCO_2 Brayton Cycle developer.
- 6.80" ID, Max P 4,000 psi, Room temp and 900°C, FoS of 1 and 2 – Based upon report by Areva in under DOE-NE in 2015 [2].
- 12.50" ID, Max P 3,675 psi, Room temp and 900°C, FoS of 1 and 2 – Based upon conceptual design study by the Black and Veatch (B&V) engineering company under DOE-EERE in 2016 [3].

For this study, MR&D began with a closed-form evaluation, the results of which are shown below in Table 17. Shown are results for a 1.0 FoS and a 2.0 FoS, where the factor was applied to the internal pressure. The results showed that a 0.199" wall thickness is required for a 1.77" ID pipe to survive a 6,200 psi pressure, a 0.471" wall thickness is required for a 6.8" ID pipe to survive a 4,000 psi pressure and a 0.791" wall thickness is required for a 12.5" ID pipe to survive a 3,675 psi pressure.

Table 17. Predictions for Three Prospective Test Cases.

		OD	ID	Outer Radius	Inner Radius	Ceramic Strength	Applied Pressure	Wall Thickness
FOS: 1.0		(in)	(in)	(in)	(in)	(psi)	(psi)	(in)
	Case #1	2.168	1.77	1.084	0.8850	30975	6200	0.199
	Case #2	7.743	6.8	3.871	3.4000	30975	4000	0.471
	Case #3	14.083	12.5	7.041	6.2500	30975	3675	0.791
		OD	ID	Outer Radius	Inner Radius	Ceramic Strength	Applied Pressure	Wall Thickness
FOS: 2.0		(in)	(in)	(in)	(in)	(psi)	(psi)	(in)
	Case 1a	2.705	1.77	1.352	0.8850	30975	12400	0.467
	Case #2a	8.857	6.8	4.428	3.4000	30975	8000	1.028
	Case #3a	15.921	12.5	7.960	6.2500	30975	7350	1.710

It was also desired to perform the same calculation for a 900°C test. According to St. Gobain [7], the flexural strength of Hexoloy SE SiC experiences a minor reduction in strength at 1450°C. Therefore, MR&D did not believe that the predictions shown in Table 17 would be significantly different for the 900°C test case.

Lastly, MR&D used the finite element model to evaluate the three (3) larger diameter multilayer samples and determine at what pressure each would fail. Table 18 shows the results of these simulations. Similar to the original correlation efforts, the finite element simulations showed that a slight improvement in pressure capability could be gained with a CMC. For these cases, MR&D defined the CMC as having four (4) +55/-55 layers with 1-lbf wind tension. As expected, the thin CMC provided more support for the smaller, thin-walled pipe.

Table 18: Predictions for Three Prospective Test Cases w/ CMC.

	Mandrel ID [in]	Mandrel OD [in]	Finished OD [in]	# Lyrs [--]	Ply Thk [in]	Angle [deg]	Tension [lbf]	SiC Final SZ [psi]	CMC Final SZ [psi]	Est P_Fail [psi]	% Failure Pressure Improvement
Case #1	1.77	2.168	2.264	4	0.012	55	1	32856.3	7111.63	6552	**5.7%**
Case #2	6.800	7.743	7.839	4	0.012	55	1	30943.4	7459.04	4104	**2.6%**
Case #3	12.500	14.083	14.179	4	0.012	55	1	34026.8	8116.82	3732	**1.6%**

5.0 Corrosion Resistance

With the assistance from Sandia National Laboratories (SNL), CTP was able to prove the corrosion resistance of two (2) types of SiC that are being considered and used in CTP's multilayer piping technology, both as the inner monolithic material. The samples were exposed to industrial-purity CO_2 at 900°C at atmospheric pressure. The tests were performed for up to 3000 hours.

CTP sent SNL sixteen (16) monolithic Hexoloy SA© and 16 (sixteen) monolithic Hexoloy SE© SiC rods (0.5" diameter, 0.75" height). Four (4) samples of each type were set aside for initial baseline characterization, and the remaining twelve (12) samples of each type were used for the long-duration compatibility testing. Industrial grade CO_2 (Matheson for Hexoloy SA© samples) was used for the compatibility experiment. Before heating the furnace, the inner quartz tube was purged with CO_2 at 200 ml/min for 12 hours to ensure that all of the air had been removed. During the experiment the CO_2 was fed at a rate of 150-200 ml/min. At 500-hour intervals, the furnace was cooled down and the weight change for all of the samples was measured. At each interval, two (2) samples were extracted for microscopic analysis.

The samples that SNL received were placed in the center of a quartz tube (1.75" OD) that was fitted inside of a high-temperature, single-zone, Lindberg-Blue tube furnace. The ends of the tube were sealed with stainless steel caps/flanges and silicone seals. A constant flow of water was maintained around the stainless-steel flanges to prevent overheating of the silicone seals.

The average SiC Hexoloy SA© sample weight change per unit surface area for 2000 hours exposure to CO_2 at 900°C is shown in Figure 38. The error bars on the graph indicate the standard deviation for the sample weight changes at each time interval. During the first 1000 hours of the test, the SiC Hexoloy SA© samples exhibited a small weight loss. This bottomed out around 1000 hours, and then began to rise up to 1500 hours, where the weight change leveled off. The same trend was observed for the SiC Hexoloy SE© samples. This trend in weight loss is very different from typically observed parabolic weight gain observed for metal alloys exposed to CO_2 at high temperatures. The magnitude of the weight change for the SiC samples is significantly lower than for metal alloys.

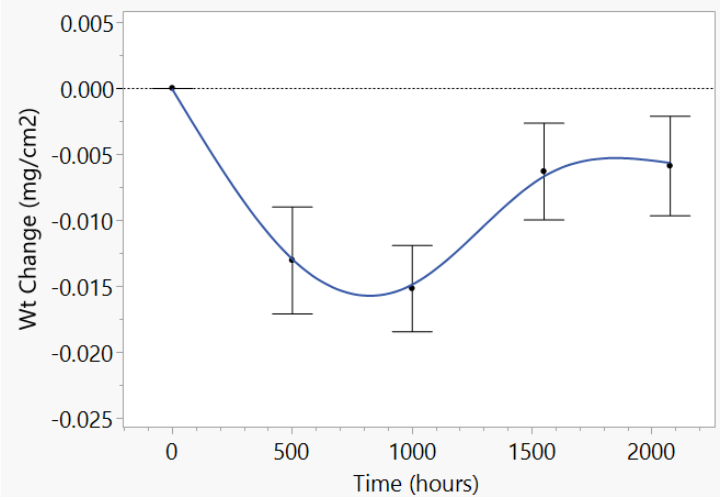

Figure 38. Average SiC Hexoloy SA© test sample weight changes during 2000 hours CO_2 exposure at 900°C Microscopy.

The surface of both an unexposed SiC Hexoloy SA© and Hexoloy SE© sample (0 hours) and for a SiC Hexoloy SA© and Hexoloy SE© sample that was exposed for 1500 hours were examined using Scanning Electron Microscope (SEM) with Energy Dispersive Spectroscopy (EDS). The results showed a significant difference in surface chemistry for the unexposed and exposed sample of both types of SiC. This difference can be seen visually (Figure 39), as samples that were exposed for longer periods were darker in color.

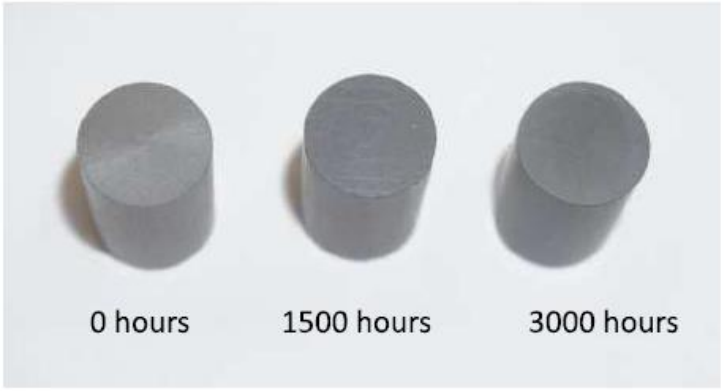

Figure 39. Color change of SiC Hexoloy SA© samples before and after CO_2 exposure.

An SEM image and measured surface chemistry for the unexposed SiC Hexoloy SA© sample and the 1500-hour exposure SiC Hexoloy SA© sample are shown in Figure 40. The surface chemistry of the two samples showed significant difference in oxygen concentration, 1.4 atom percent for the unexposed sample and 36 atom percent for the exposed sample.

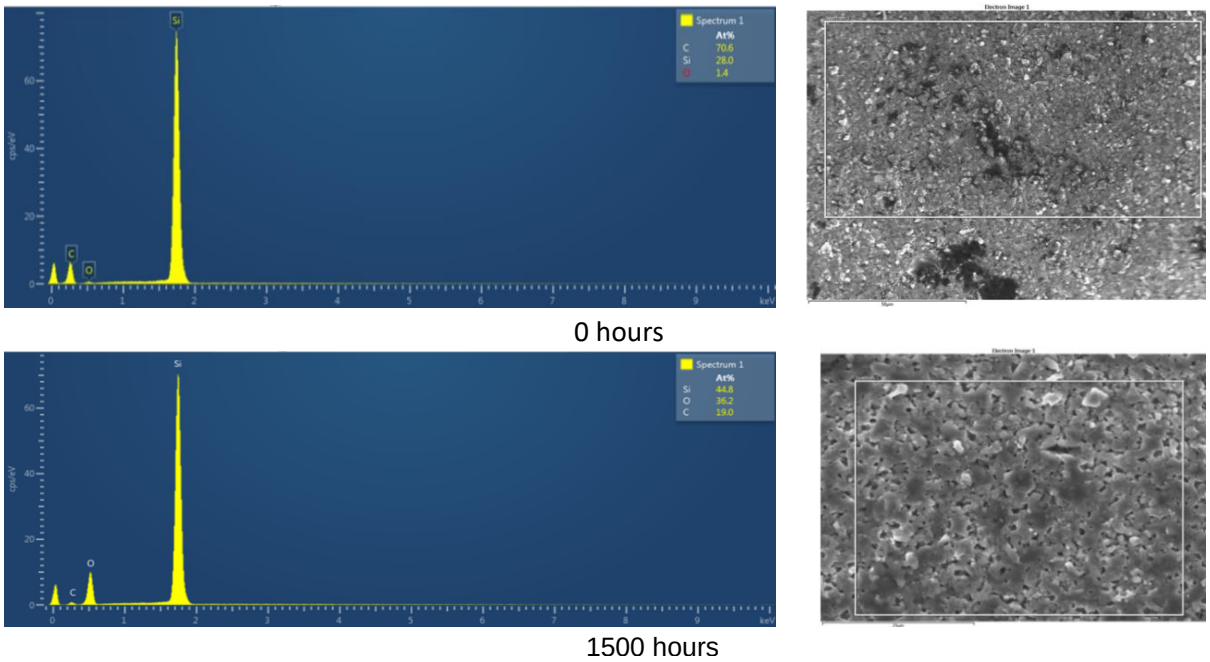

Figure 40. SEM and EDS surface chemistry for an unexposed (0 hours) SiC Hexoloy SA© sample and exposed (1500 hours) SiC Hexoloy SA© sample.

The observed differences in surface chemistry suggest that exposure of the SiC samples to high-temperature CO_2 results in the formation of an oxide-rich layer on the samples' surface, as was also oberserved on the SiC Hexoloy SE© samples. This surface oxide is not evident in the SEM images for the samples not exposed to CO_2. Visual observation of the exposed sample shows the presence of light and dark regions along the length of the exposed surface. These bands were not present on the surface of the unexposed sample.

To determine the nature of the surface oxide of the exposed samples, including the discolored bands, cross-sectional samples were prepared for several samples (0 hours, 1500 hours, and 2000 hours) in an FEI Helios 660 Nanolab focused ion beam (FIB). A platinum (Pt) coating was applied to the sample surface prior to the extraction of the cross-sectional sample to protect the sample surface during the extraction. A cross-sectional image and the presence of oxygen for the unexposed sample is shown in Figure 41.

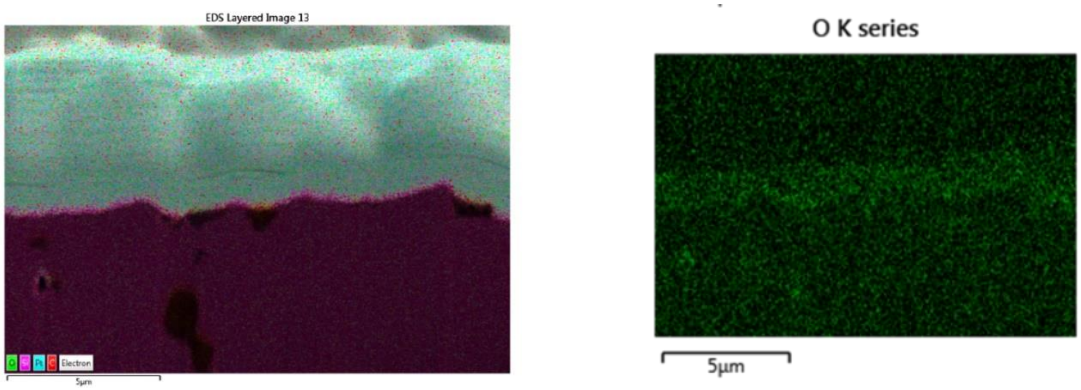

Figure 41. Oxygen concentration in an unexposed SiC Hexoloy SA© sample.

Cross-sectional samples were prepared for both the light and dark colored regions of a 1500-hour sample and a 2000-hour sample. A comparison of the oxygen concentration of light and dark areas for the two exposed samples is shown in Figure 42.

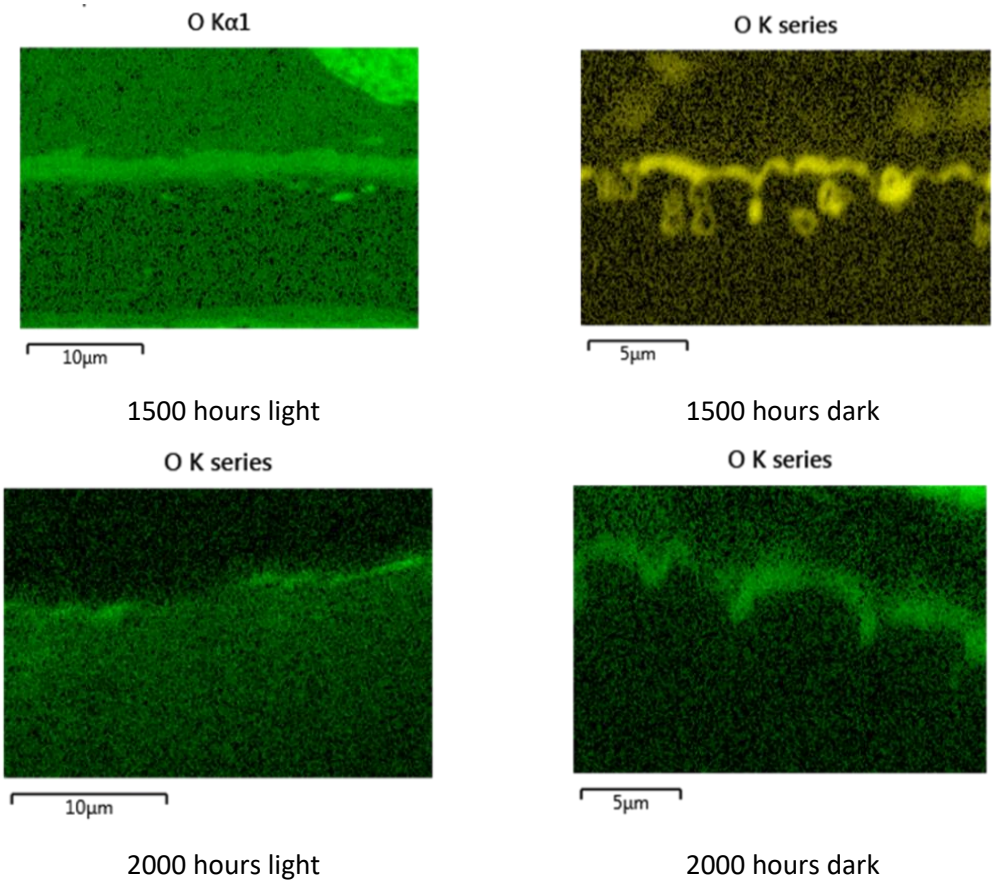

Figure 42. Comparison of oxygen concentration in light and dark areas of the 1500- and 2000-hour SiC Hexoloy SA© samples.

The analysis of the light-colored area shows a uniform layer of oxide (2-3 microns thick). The oxide layer was also observed for the dark colored are, but it was much thinner. The oxide layer of the light area for the 2000-hour sample appears different from that of the 1500-hour sample. No distinct oxide layer is present at the surface, but the concentration of oxygen appears higher in the material relative to concentration of carbon. The dark colored region does show a uniform layer of oxygen rich material (2-3 microns) at the sample surface.

The observed differences in the samples were surprising, considering there were very minor average weight changes between the two samples. It appears that change in the nature, not the thickness, of the surface oxide coating is occurring after 1500 hours exposure.

SiC Hexoloy SE© samples had a similar oxide growth as the SiC Hexoloy SA© samples. The oxide thickness increased from approximately 0.5 micrometers at 1500 hours, to 2.5 and 3 micrometers at 3000 hours (two locations were analyzed for the 3000-hour case). Top-down images of the SiC Hexoloy SE© samples are shown in Figure 43, while cross-sectional images are provided in Figure 44.

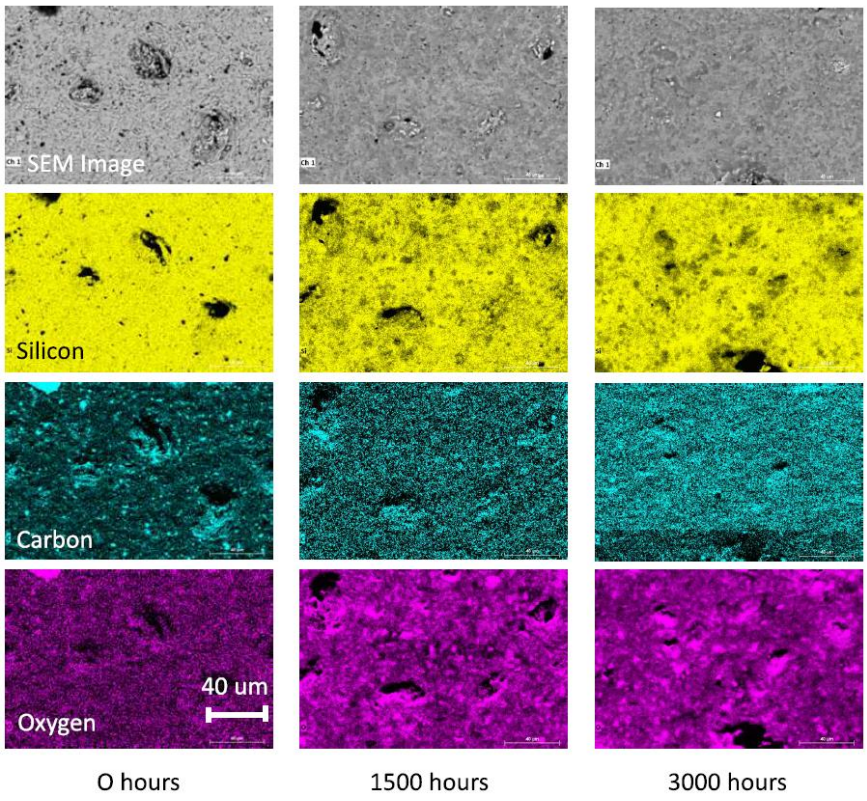

Figure 43. Top-down SEM/EDS images of the SiC Hexoloy SE© surface after 0, 1500, and 3000 hours of CO_2 showing a noticeable increase in oxygen with exposure time.

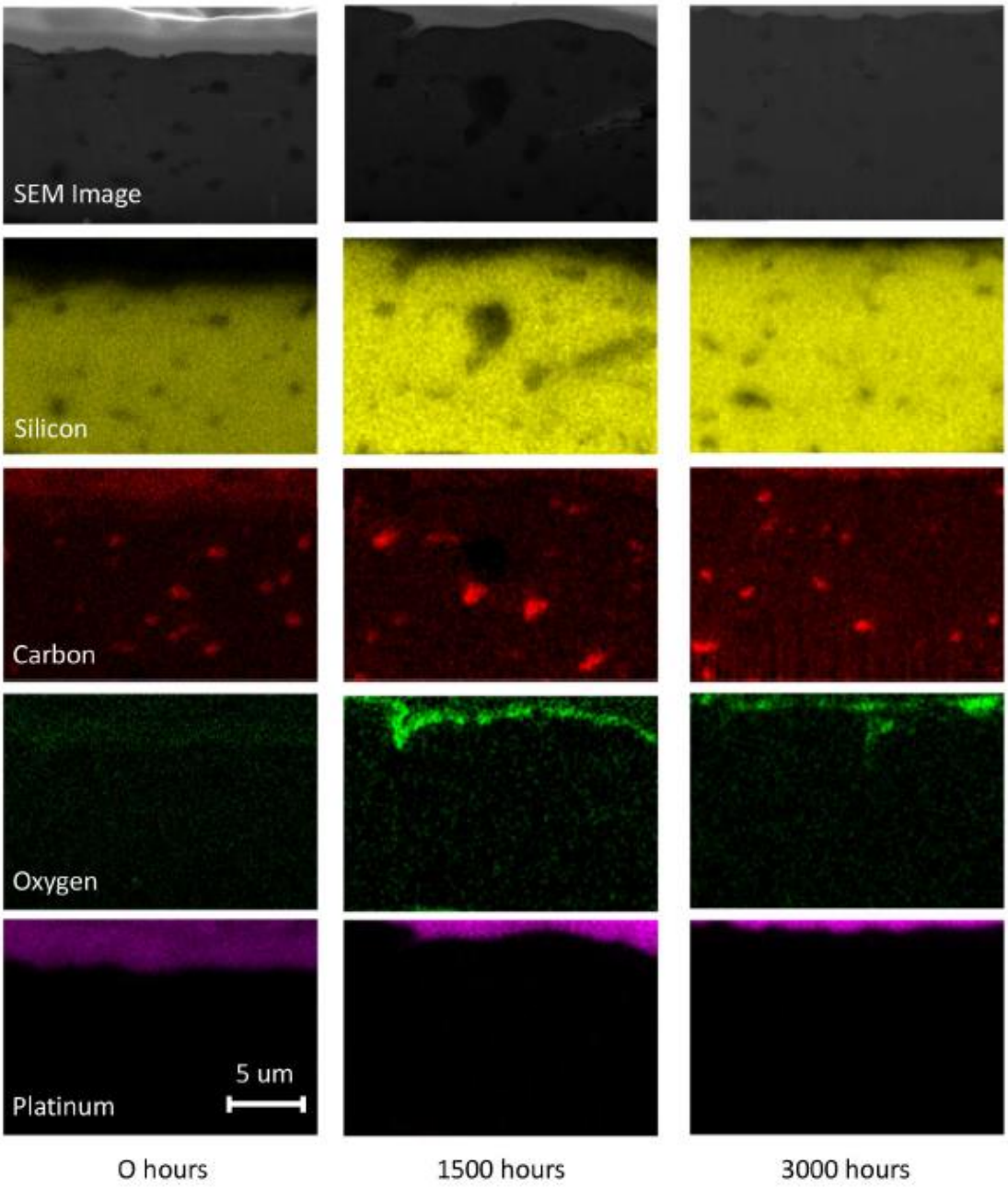

Figure 44. Cross-sectional SEM/EDS images near the SiC Hexoloy SE© surface after 0, 1500, and 3000 hours of CO_2 exposure. The concentration of oxygen increased with exposure time.

Prior experiments were conducted at the University of Wisconsin (UW) to understand the removal of carbon from metal carbide typically present in steel alloys. The results from this test, including results for the chemical compatibility of SiC with sCO_2, were reported by Sridharan [4]. For these tests, SiC samples were exposed to different purities of sCO_2 at 650°C and 750°C. The experiments used higher-purity Research Grade (RG) and lower-purity Industrial Grade (IG) CO_2. In all four cases, the SiC samples experienced an initial weight loss followed by weight gains. Despite the different experimental conditions, these results mimic the results from the tests at Sandia. The results obtained from the tests at Sandia (in purple) are shown in combination with the results from UW in Figure 45.

A significantly larger initial weight loss was observed for the Wisconsin samples, than for the Sandia samples. Another observation was the greater initial weight loss for the Wisconsin samples exposed to IG CO_2 versus those exposed to RG CO_2.

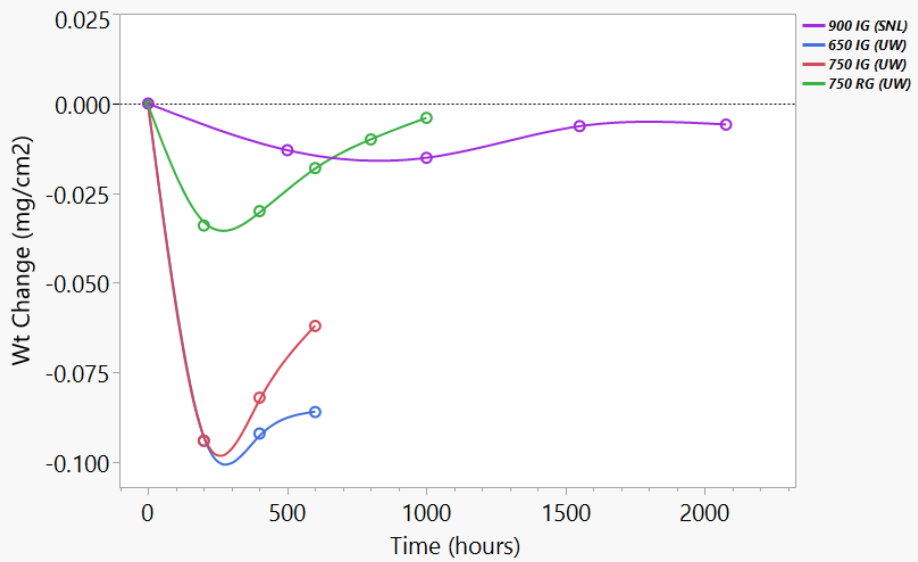

Figure 45. Weight change for SiC samples exposed to RG and IG CO_s gases at Wisconsin (UW, sCO_2) and Sandia (SNL, CO_2).

Sridharan hypothesized that the initial weight loss was due to the reaction of CO_2, and its impurities, with SiC, resulting in the formation of carbon monoxide (CO) and a Si-rich surface layer. After the initial weight loss, the Si-rich surface layer reacted with CO_2 to form a silicon dioxide (SiO_2) passivation layer. The creation of this layer contributed to the sample weight gain and eventual leveling off of weight change for the samples. Evidence of this hypothesis is provided in the reaction of CO_2 with graphite that was identified in a separate set of experiments.

In a different study, Opila [12], evaluated the oxidation of very-high-purity (99.999%) chemically-vapor-deposited (CVD) SiC in high-temperature, 1200-1400°C, high-purity CO_2. No initial weight loss was observed during these tests. Instead, the samples demonstrated very small weight gains during 100-hour exposure. They describe the following reaction as taking place:

$$SiC + 3\ CO_2\ (g) = SiO_2 + 4\ CO\ (g)$$

This reaction would result in an overall weight gain for the sample instead of weight loss.

A key difference between the two studies was the purity of the reactants in the system. The report by Sridharan does not provide the purity of SiC samples that were used, but it is likely they were less pure than the material used by Opila, and possibly less pure than the SiC used at Sandia. From this information, a new hypothesis has been developed. Impurities that are present in the CO_2 or SiC react within the system causing the initial weight loss. Over time a layer of SiO_2 forms on the surface of the SiC and a weight gain is observed. This layer thickens until it provides a barrier against further reaction between the CO_2 and SiC and their impurities. Support for this hypothesis is observed in the greater initial weight loss among the Wisconsin samples in IG sCO_2 versus RG sCO_2. If the Sandia test samples are, in fact, higher purity than the Wisconsin test samples, the higher initial weight loss for the Wisconsin samples would support this hypothesis.

Regardless of the cause of the weight change behavior in high-temperature CO_2, SiC has been demonstrated as being very stable in this environment. The weight change exhibited during 2000 hours exposure in 900°C sCO_2 is negligible. A thin, dense protective layer of SiO_2 oxide appears to form on the surface, minimizing the degradation of the material in this environment. Overall, SiC has demonstrated excellent chemical compatibility in high-temperature CO_2 environments.

For comparison, the minimal weight change behavior for SiC in CO_2 is graphed alongside that of high-temperature Ni-based alloys (230, 282, 740H) in Figure 46. The weight gains for the Ni-base alloys are significantly higher than that for SiC at 900°C. This comparison further supports SiC as an excellent alternative to Ni-based alloys for high-temperature sCO_2 piping applications.

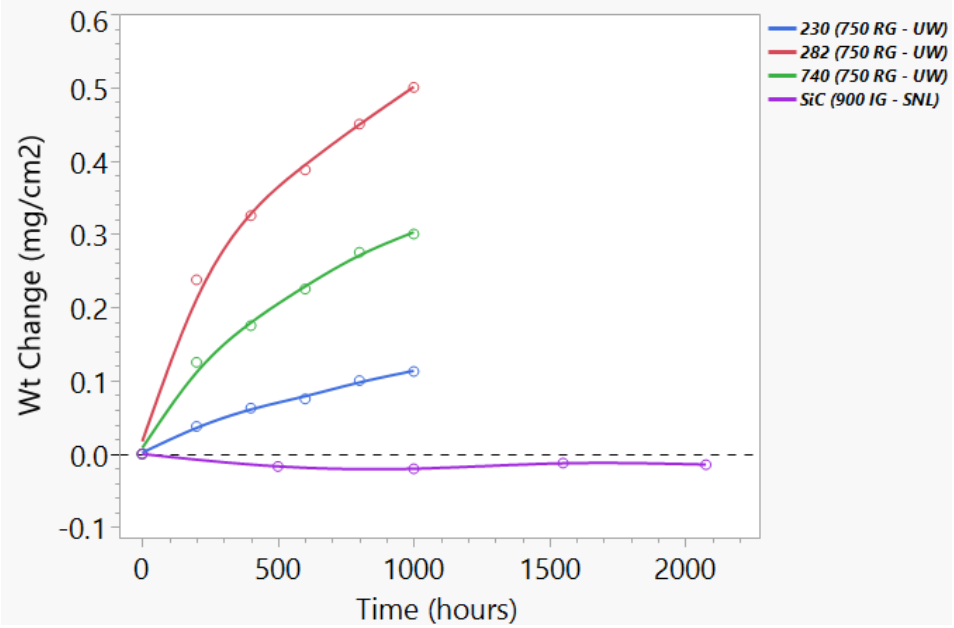

Figure 46. Weight change comparison for SiC and Ni-base alloys in high temperature CO_2.

6.0 Conclusion

The multilayer technology that CTP has been developing has a number of advantages, several of which were discussed in the above sections, over conventional and nickel-based alloys. At temperatures up to and well above 700°C multilayer pipes offer a hermetic, corrosion resistant, and tough piping solution able to retain high pressures over an extended period of time. Using the finite element model that MR&D has developed, CTP is able to optimize the component parts of the multilayer design to better utilize materials and reduce cost. Additionally, high temperature CO_2 does not negatively affect the performance of both varieties of the inner monolithic SiC that were examined during this study. Overall, when high operating temperatures (>700°C) and/or pressures (>1000 psi) are needed, as is the case for some unregulated sCO_2 and next generation sCO_2 Brayton power cycles, advanced heat exchangers, and CSP receivers, multilayer components provide unmatched performance in key areas over traditional and nickel-based alloys.

CTP continues to refine its technology and to perform testing and data analyses necessary to attain high-level confidence in its products. This will include continued proactive engagement with technology developers to explore opportunities for collaboration in future testing.

Acknowledgement

The author would like to acknowledge the support of the U.S. Department of Energy for funding this research under contract DE-SE00018733. Special thanks to Matthew Walker and Arthur Kariya of Sandia National Laboratories for performing the chemical compatibility testing presented.

References

[1] K. Brun, P. Friedman and R. Dennis, "Fundamentals and Applications of Supercritical Carbon Dioxide (sCO_2) Based Power Cycles," Woodhead Publishing, 2017, ISBN 978-0-08-100804

[2] AREVA, "Task Order 20: Supercritical Carbon Dioxide Brayton Cycle Energy Conversion Study - Final Report - RPT – 3011934-000," 2015.

[3] Black & Veatch, "Supercritical Carbon Dioxide Power Generation System Definition - Concept Definition and Capitol Cost Estimate," June 2016.

[4] K. Sridharan, “Corrosion of Structural Materials for Advanced Supercritical Carbon-Dioxide Brayton Cycle”, US DOE NEUP Project Final Report, Project # 13-4900, 2017.

[5] "Concise Encyclopedia of Advanced Ceramic Materials," pp. 488-494, 1991.

[6] J. Green, "Types and Applications of All Kinds of Ceramic Materials in 2021," Advanced Ceramic Materials, 2021. [Online]. Available: https://www.preciseceramic.com/blog/types-and-applications-of-all-kinds-of-ceramic-materials/. [Accessed 2021].

[7] Saint-Gobain Ceramics, "Hexoloy SE Silicon Carbide - Technical Data," 2012.

[8] Y. Katoh and L. Snead, "Silicon Carbide and its Composites for Nuclear Applications – Historical Overview," vol. 526, no. 151849, 2019.

[9] H. Zhang and R. P. Singh, "Novel Processing of Unique Ceramic-Based Nuclear Materials and Fuels," Oklahoma State University, No. DOE/ID/14673.2008.

[10] L. Menachem and J. Preston, "Handbook of Fiber Science and Technology. Vol. III. High Technology Fibers, Part C." *Dekker, Marcel, Inc, P. O. Box 5005, Monticello, NY 12701-5185, USA, 1993. 408* (1993).

[11] T. W. Clyne and D. Hull, An Introduction to Composite Materials, Cambridge University Press, 2019.

[12] E. Oplia and Q. Nguyen, "Oxidation of Chemically-Vapor-Deposited Silicon Carbide in Carbon Dioxide," Journal of the American Ceramic Society, 81, 1998.